DTIC
ELECTE
AUG 31 1993
S D
C

AD-A268 645

SC71040.FR

Copy No. 4

AFOSR-TR- 93 0650

INTEGRATION OF FERROELECTRIC/SEMICONDUCTOR THIN FILMS FOR SLM AND PHOTOREFRACTIVE APPLICATIONS

FINAL REPORT

September 24, 1990 through March 23, 1993

CONTRACT NO. F49620-90-C-0084

Prepared for:

Air Force Office of Scientific Research
Bolling AFB
Washington, DC 20332

Prepared by:

R.R. Neurgaonkar
Principal Investigator

August 1993

Approved for public release; distribution unlimited

"The views and conclusions contained in this document are those of the authors and should not be interpreted as necessarily representing official policies, either expressed or implied, of the Defense Advanced Research Projects Agency or the U.S. Government."

Rockwell International
Science Center

93-20273

93 8 30 036

UNCLASSIFIED

SECURITY CLASSIFICATION OF THIS PAGE

REPORT DOCUMENTATION PAGE

FORM APPROVED OMB No. 0704-0188

1a. REPORT SECURITY CLASSIFICATION
Unclassified

1b. RESTRICTIVE MARKINGS

2a. SECURITY CLASSIFICATION AUTHORITY

3. DISTRIBUTION/AVAILABILITY OF REPORT
Approved for public release; distribution is unlimited.

2b. CLASSIFICATION/DOWNGRADING SCHEDULE

4. PERFORMING ORGANIZATION REPORT NUMBER(S)
SC 71040

5. MONITORING ORGANIZATION REPORT NUMBER(S)

6a. NAME OF PERFORMING ORGANIZATION
Rockwell International Science Center

6b. OFFICE SYMBOL (If Applicable)

7a. NAME OF MONITORING ORGANIZATION
AFOSR/NE

6c. ADDRESS (City, State and ZIP Code)
1049 Camino Dos Rios
Thousand Oaks, CA 91360

7b. ADDRESS (City, State and ZIP Code)
110 Duncan Suite B115
Bolling AFB DC 20332

8a. NAME OF FUNDING/SPONSORING ORGANIZATION
Same as 7a

8b. OFFICE SYMBOL (If Applicable)
NE

9. PROCUREMENT INSTRUMENT IDENTIFICATION NUMBER
Contract No. F49620-90-C-0084

8c. ADDRESS (City, State and ZIP Code)
Same as 7b

10. SOURCE OF FUNDING NOS.

PROGRAM ELEMENT NO.	PROJECT NO.	TASK NO.	WORK UNIT ACCESSION NO.
61102F	Darpa		

11. TITLE (Include Security Classification)
Integration of Ferroelectric/Semiconductor Thin Films for SLM and Neural Network Applications

12. PERSONAL AUTHOR(S)
Neurgaonkar, Ratnakar R.

13a. TYPE OF REPORT	13b. TIME COVERED	14. DATE OF REPORT (Year, Month, Day)	15. PAGE COUNT
Final Report	FROM 09/24/90 TO 03/23/93	1993, August 9	

16. SUPPLEMENTARY NOTATION
Reproduction in whole or in part is permitted for any purpose of the US Government.

17. COSATI CODES			18. SUBJECT TERMS (Continue on reverse if necessary and identify by block number)
FIELD	GROUP	SUB-GROUP	Grain-oriented thin films, sol-gel, sputtering, PLZT and SBN thin films. Spatial light modulator (SLM), guided wave optics, and optical data storage.

19. ABSTRACT (Continue on reverse if necessary and identify by block number)

In order to achieve high optical modulation in SLM applications, we have successfully fabricated multilayer stacks of thin films consisting of PLZT and SBN, using the sol-gel and sputtering deposition techniques. The performance of these multilayer devices is excellent. In another approach, doped grain oriented PLZT and $BaTiO_3$ thin films have been fabricated on SBN substrates. Because of the availability of such high performance films, various applications in the areas of SLM, guided-wave optics and optical data storage are emerging for these films.

20. DISTRIBUTION/AVAILABILITY OF ABSTRACT
Same as report

21. ABSTRACT SECURITY CLASSIFICATION
Unclassified

22a. NAME OF RESPONSIBLE INDIVIDUAL
Craig

22b. TELEPHONE NUMBER (INCLUDE AREA CODE)
202-767-4931

22c. OFFICE SYMBOL
NE

DD FORM 1473 Previous editions are obsolete.

UNCLASSIFIED

SECURITY CLASSIFICATION OF THIS PAGE

TABLE OF CONTENTS

DTIC QUALITY INSPECTED 3

Accesion For
NTIS CRA&I
DTIC TAB
Unannounced
Justification
By
Distribution /
Availability Codes
Dist | Avail and / or Special
A-1

LIST OF FIGURES

LIST OF TABLES

1.0 ABSTRACT

This report covers work on the integration of ferroelectric and semiconductor materials for SLMs carried out over the period of September 24, 1990, through March 23, 1993, in the Ferroelectric Materials Department of the Rockwell International Science Center under Contract No. F49620-90-C-0084. During this period, significant progress has been made in the growth of highly grain-oriented perovskite PZT and $BaTiO_3$ thin films on lattice matched SBN, $SrTiO_3$ and MgO substrates. The oriented PZT films show high polarization in the range of 30 - 38 $\mu coul/cm^2$, indicating the strong electro-optic effect necessary for photorefractive applications. This report also includes the growth of individual PZT and SBN:75 thin films on semiconducting Si substrates and the successful fabrication of ferroelectric multilayers consisting of alternating PZT and SBN films for spatial light modulators (SLMs).

Because excellent quality and optical property PZT, $BaTiO_3$ and multilayer (consisting of PZT and SBN) films are now available, a wide range of optical devices are currently under investigation. Under this program, we are concentrating SLM applications at UCSD using the multilayer stack films; while photorefractive applications are being developed at Rockwell using the grain-oriented PZT and $BaTiO_3$ films deposited on SBN substrates.

2.0 INTRODUCTION

The objective of the this program was to integrate ferroelectric and semiconductor materials for applications in spatial light modulators (SLMs) and photorefractive applications. These devices may include image processing, photorefractive channel waveguides, optical signal filters, optical neural computing and other types of devices. The development of ferroelectric thin films for SLM and photorefractive applications is summarized in Figure 2.1

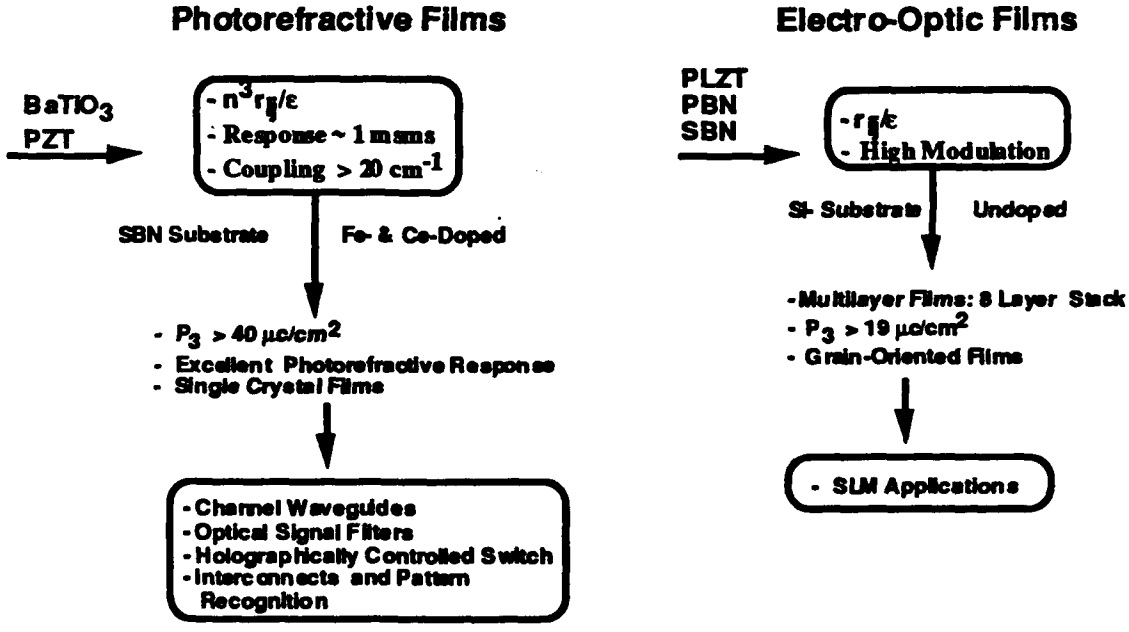

Figure 2.1 -- The development of ferroelectric thin films for SLM and photorefractive applications.

Using techniques that have become well established at Rockwell, the fabrication of ferroelectric thin films grown on various substrates has been carefully studied with respect to film growth conditions, annealing temperature, substrate type and substrate orientation. After the samples are thoroughly characterized by our group, structures fabricated under this program are being evaluated at the University of California, San Diego (Professor Sing Lee) and at the Rockwell International Science Center (Dr. John Hong) for possible use in the specific devices mentioned above.

3.0 PROGRESS SUMMARY AND MAJOR ACCOMPLISHMENTS

Table 3.1 summarizes the ferroelectric thin film materials selected for study under this program. The optical figures-of-merit for these materials are exceptionally good and currently we have established the sputtering and sol-gel growth techniques for PZT and SBN compositions. In our earlier experiments, we used tungsten bronze PBN:60 for the development of multilayer film stacks; however, our work shows that PZT and PBN react at elevated temperatures and only the tungsten bronze phase is crystallized. For this reason, we have selected PZT and SBN:75 for the multilayer stack work, where they have been grown individually and as alternating layers.

Table 3.1
Comparison of PLZT, SBN and KTN Materials
(assuming E = 2V/μm)

PLZT	SBN 75	KTN
$\Delta n = \frac{n^3 R E^2}{2}$	$\Delta n = .5(n_e^3 r_{33} - n_0^3 r_{13})E$	$\Delta n = .5(n_e^3 r_{33} - n_0^3 r_{13})E$
$\Delta n = 11 \times 10^{-3}$	$\Delta n = 1.63 \times 10^{-2}$	$\Delta n = 8.72 \times 10^{-3}$
$\varepsilon_r = 4500$	$\varepsilon_{33} = 3000$	$\varepsilon_{33} = 2000$
$\frac{\Delta n}{\varepsilon E^2} = 6.1 \times 10^{-19}$	$\frac{\Delta n}{\varepsilon_{33} E^2} = 1.4 \times 10^{-18}$	$\frac{\Delta n}{\varepsilon_{33} E^2} = 2.7 \times 10^{-19}$

Table 3.2 summarizes the development of ferroelectric thin film structures for spatial light modulators (SLMs) and optical information processing systems (photorefractive effects) that has been proceeding at Rockwell International over the past 30 months. Substantial progress has been made in establishing the best compositions and deposition conditions for electro-optic and photorefractive films using various substrates appropriate for each application. For SLMs, the most significant accomplishment has been the deposition of alternating PZT and SBN:75 layers on Pt-coated Si substrates.

Table 3.2
Integration of Ferroelectric Films with Different Substrate Materials

Film Composition and substrates	Crystallinity	Dielectric Constant ε	Polarization ($\mu coul/cm^2$)	Applications
PZT Films				
Si or GaAs	Partially Oriented	1100-1200	> 15	SLMs
(100) $SrTiO_3$	Partially Oriented	-----	-----	Photorefractive
(001) SBN:60	Single Crystal	1200-1400	> 20	Photorefractive
$BaTiO_3$ Films				
(001) SBN:60	Single Crystal	>3000	-----	Photorefractive
PBN:60 Films				
Si or GaAs	Partially Oriented	>900	> 20	SLMs
(001), (100) SBN	Single Crystal	-----	-----	Photorefractive
SBN Films				
(001) & (100) SBN	Single Crystal	-----	-----	Photorefractive
Si	Highly Oriented	~600	> 8	SLMs

All photorefractive films are doped with Ce^{3+} or Fe^{3+}

In the case of photorefractive films, we are the first group to deposit nearly single crystal PZT

and $BaTiO_3$ thin films on lattice-matched SBN:60. These films contain dopants suitable for controlling photorefractive speed, coupling and diffraction efficiency. This work forms a basis for the development of specific device concepts. At UCSD, Professor Sing Lee and his group have formulated several structural designs for SLMs based on our electro-optic multilayer thin film structures. At the Rockwell International Science Center, John Hong is also generating designs for various optical information processing functions using these photorefractive films.

3.1 Electro-Optic Thin Films for SLMs

The main objective for this task was to achieve high electro-optic response films operating at low voltages. For this task we selected PZT/PLZT, PBN:60 and SBN:75 because they possess outstanding electro-optic properties (Table 3.1) and because we expected that these materials could be made compatible with one other and with the substrates.

3.1.1 Single Layer Electro-Optic Films

We optimized the film growth conditions for PZT, PLZT, PBN:60 and SBN:75 on Pt-coated Si substrates, and found that highly grain-oriented films of the tungsten bronze compositions could be obtained when the substrate temperature was kept above 400 °C during film growth (sputtering technique). Figure 3.1 shows x-ray diffraction patterns for partially and fully oriented SBN:75 on Si. The remanent polarization in the films was over 15 $\mu coul/cm^2$ indicating large electro-optic effects are possible in these films.

3.1.2 Multilayer Films

The structure shown in Fig. 3.2, consisting of two ferroelectric layers deposited on Pt-coated Si substrates, has been successfully fabricated using PZT and SBN:75. The x-ray diffraction pattern shown in Fig. 3.3 indicates that both layers are crystalline with the desired perovskite and tungsten bronze structures. In this example, PZT was first deposited on Si by the sol-gel technique and then followed by the deposition of SBN:75 by the magnetron sputtering technique. Figure 3.4 shows the polarization behavior measured for this combined multilayer stack. The results are

highly promising and support the multilayer concept for SLMs. The magnitude of the remanent polarization is sufficiently high in the multilayer stack, and this will improve significantly when the grains in these films are fully oriented. Currently, efforts are underway to orient the PZT grains by using the oriented electrode layers between film and substrate. The succeeding ferroelectric SBN and PZT layers grown on such substrate will maintain high degree of orientation.

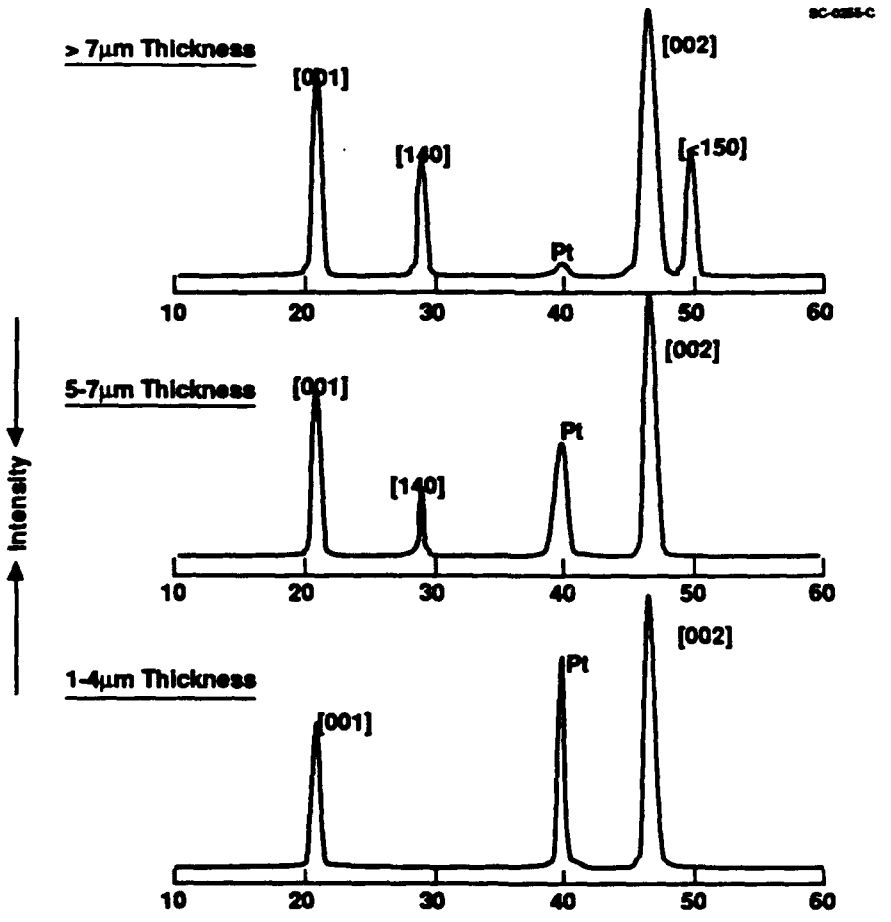

Figure 3.1 -- Grain-orientation in SBN:75 films as a function of thickness.

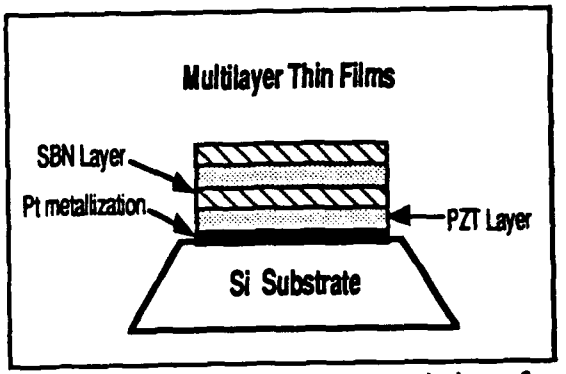

Figure 3.2 – SLM structure consisting of two ferroelectric layers deposited on Si.

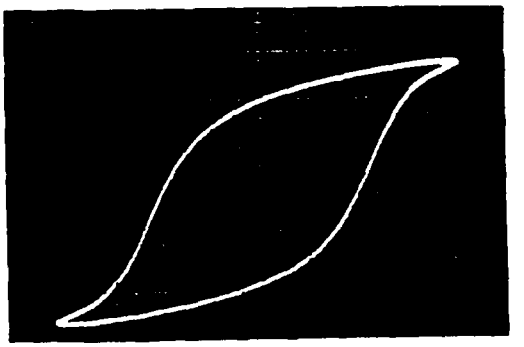

Figure 3.4 – Hysteresis loop of multilayer PZT/SBN films on Pt/Si substrate.

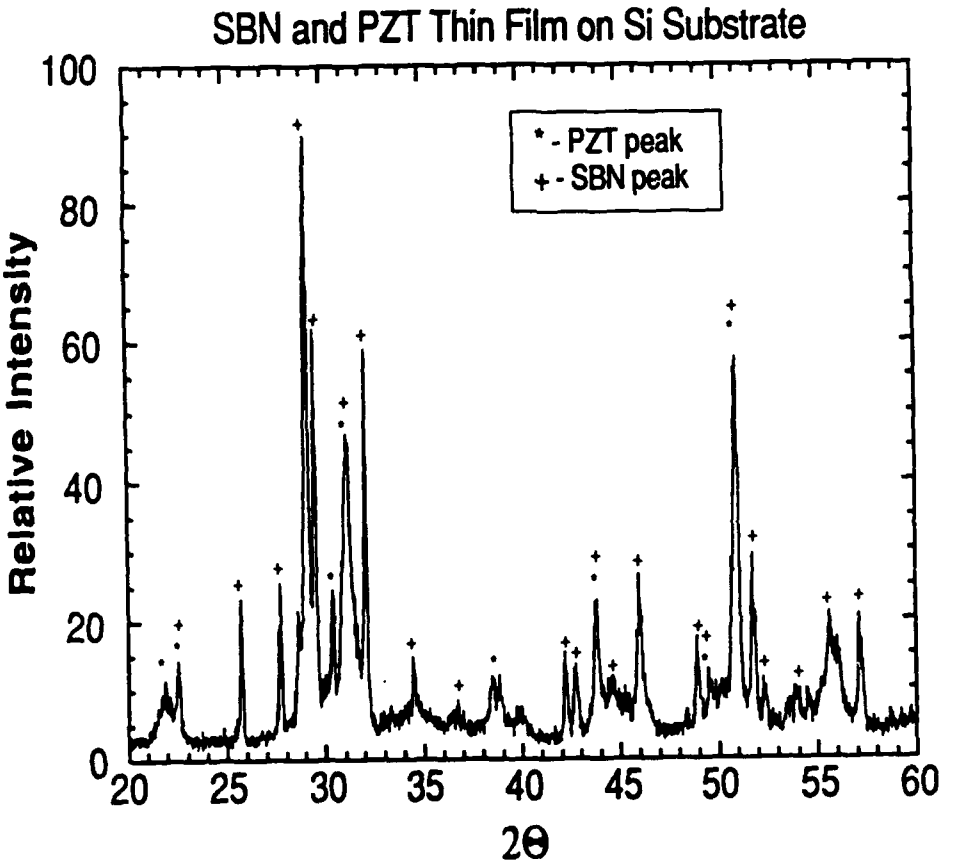

Figure 3.3 – X-ray diffraction pattern for multilayer PZT/SBN films.

We systematically studied our films using various structural and ferroelectric measurement techniques on single layers as well as on multilayer stacks. The results of this work are summarized below:

Property	SBN	PZT	PZT/SBN
T_c (°C)	58	~150	---
Dielectric Constant	1000	1400	1100
Polarization ($\mu c/cm^2$)	~7	>19	~15
Electro-Optic Coefficient (x 10^{-12} m/V)*	>140	>470	~300
Piezoelectric Coefficient	>75	>230	~15

* Electro-optic coefficients were established using dielectric and polarization values

These properties are promising and can be further improved by achieving a higher degree of grain orientation, specifically in the SBN films. Since only two poling directions are available in tetragonal SBN, a higher field is required to pole these films. In order to improve the grain-orientation in SBN films, we have deposited SBN films on Si substrates having different electrode materials such as Platinum (Pt), Gold (Au) and $Sr_{0.5}La_{0.5}CoO_3$ (LSC). Our work indicates that LSC is the choice of best electrode materials in order to improve the grain orientation in the films. In our future work, we will continue to include both LSC and Pt electrodes for ferroelectric films development.

3.2 Photorefractive Films

3.2.1 Growth of PZT Films

For photorefractive applications, one needs highly grain-oriented films, doped with suitable dopant(s), where no electric field is required to utilize the photorefractive effect. Since SBN has an excellent lattice-match with both PZT and $BaTiO_3$, we have exploited SBN as a substrate material

for the growth of these high optical figure-of-merit films. The films have been grown by the sol-gel technique and the details of our growth are as follows:

Film Composition:	PZT (60:40) and $BaTiO_3$
Substrate:	(001)-Oriented SBN:60 and SBN:50, MgO and $SrTiO_3$
Dopants:	Fe^{2+}/Fe^{3+} and Ce^{3+}/Ce^{4+}
Annealing Temperature:	(a) 650°C for PZT (b) 750°C for $BaTiO_3$
Film Thickness:	(a) 2-3 μm for PZT films (b) 3-5 μm for $BaTiO_3$ films

Table 3.3 summarizes growth conditions for the PZT films and the results of each growth in terms of film thickness and degree of orientation. The most extensive set of growth experiments was carried out on SBN substrates. These included two different substrate orientations with no buffer layer and conducting LSC buffer layer. The conducting buffer layer allows direct measurements of the ferroelectric properties of the PZT films.

As shown by the x-ray diffraction patterns in Fig. 3.5, the PZT films deposited on [001] SBN:60 substrates are highly oriented along the [100] direction of the perovskite structure because of the close lattice match between [100] PZT and [001] SBN:60. This is the first time the sol-gel process has been successfully used to grow highly grain-oriented PZT films on SBN. Since the refractive index difference between PZT and SBN:60 is large ($\Delta n \sim 0.218$), this structure could have a significant impact on photorefractive and electro-optic applications. We are currently adjusting the film composition to improve the lattice match with SBN:60, which will lead to lower strain and fewer defects in the films. In contrast, PZT films grown on [100]-oriented SBN:60 substrates are typically lattice-mismatched and therefore the films are polycrystalline with no preferred orientation.

Also shown in Fig. 3.5 is the diffraction pattern for PZT grown on SBN/LSC. The LSC buffer layer grows on SBN:60 as a highly oriented cubic perovskite with a lattice constant slightly lower than the c-axis value for SBN. For this reason, the subsequent PZT layer also achieves good grain orientation.

Table 3.3
Growth Conditions for PZT Films

Substrate	Annealing Temp (°C)	Thickness (μm)	Film Orientation	Unit Cell (Å)
SBN Substrate				
(001) No Coating	640-675	0.5 to 1.5	(100) oriented	4.015
(001) LSC-Coating	620-640	0.5 to 1.0	(100) oriented	4.021
(100) No Coating	640-675	0.5 to 1.0	polycrystalline	----
$SrTiO_3$ Substrate				
(100) No Coating	620-635	0.5 to 1.0	(100) oriented	3.992
(100) LSC Coating	620-635	0.5 to 1.2	(100) oriented	3.995
MgO Substrate				
(100) No Coating	640-650	0.5 to 1.0	partially oriented	4.081
(100) LSC Coating	640-650	0.5 to 1.0	(100) oriented	4.081

Figure 3.6 shows the x-ray diffraction patterns for grain-oriented PZT films on LSC coated $SrTiO_3$ and MgO substrates. Since the film, substrate and buffer layers are all perovskite, we expected that the crystallinity of the PZT films on $SrTiO_3$/LSC should be good. It has been reported that single crystal PZT films have been grown by rf sputtering on [100]-oriented $SrTiO_3$ substrates for optical applications, but this is the first instance of sol-gel growth of such films. Efforts are under way to study the film quality for optical applications using [110] and [111]-oriented $SrTiO_3$ substrates.

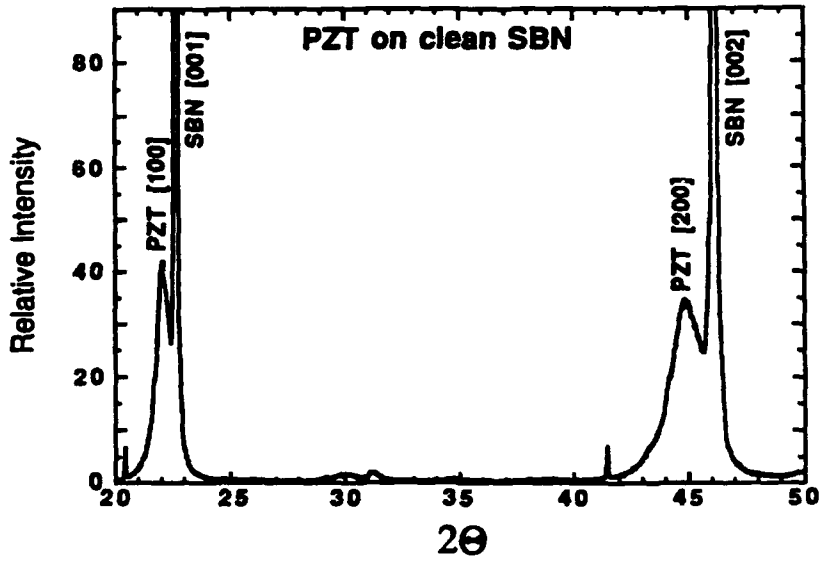

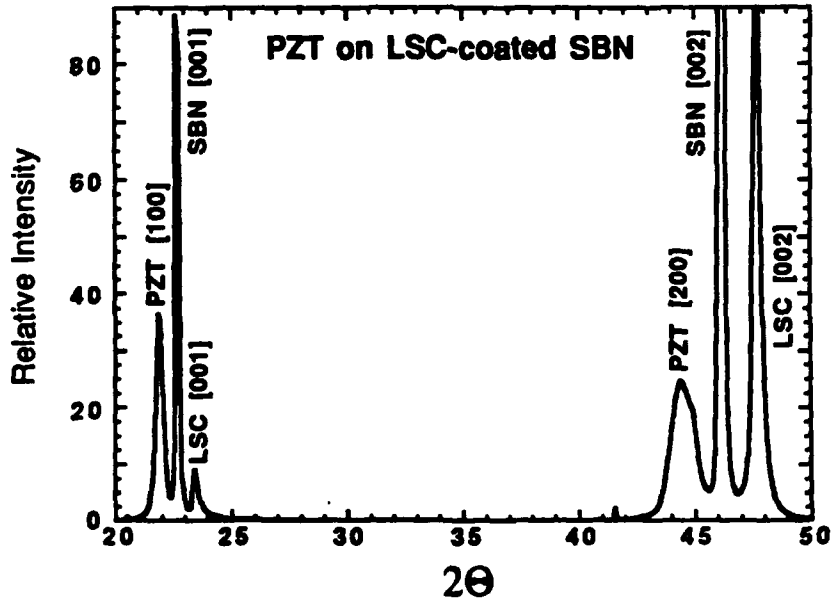

Figure 3.5 -- X-ray diffraction pattern of PZT films on clean and LSC-coated SBN substrates.

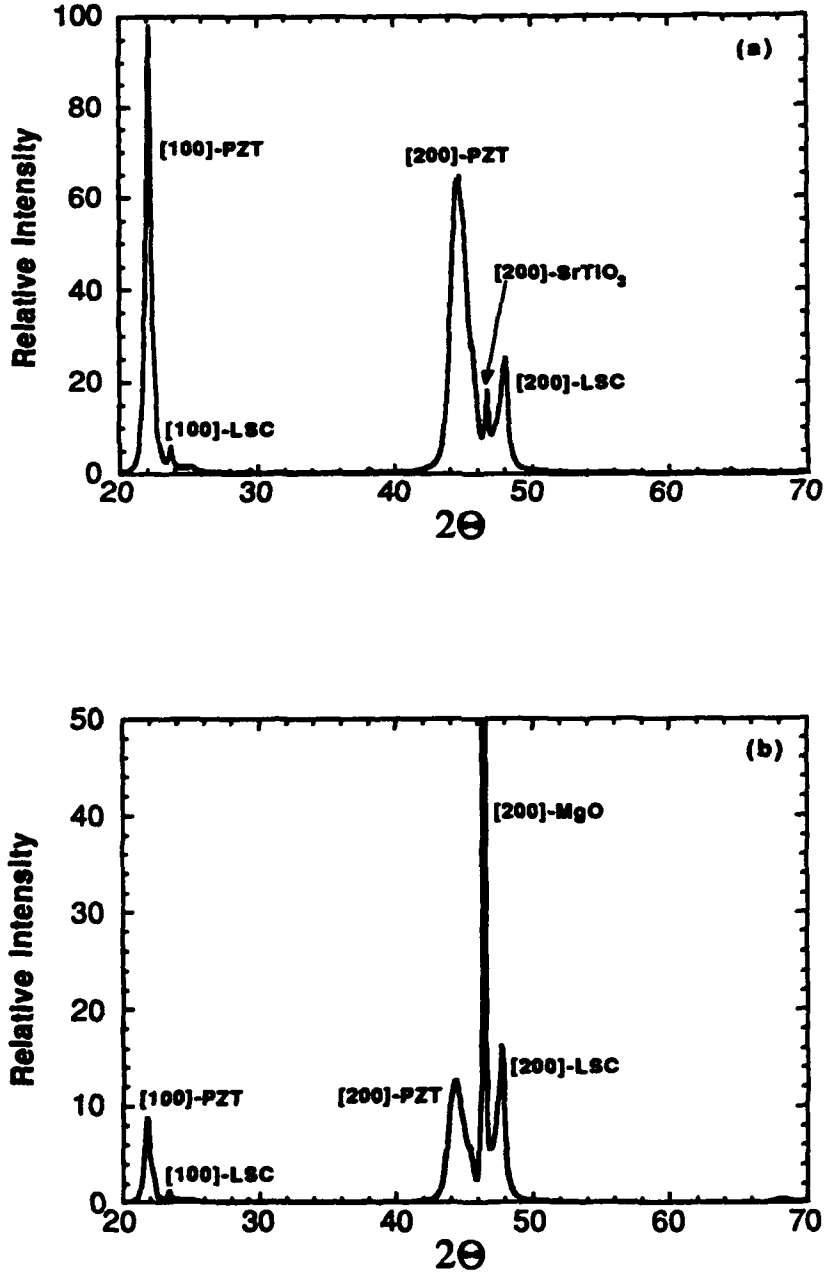

Figure 3.6 -- X-ray diffraction patterns for PZT films on (a) $SrTiO_3$ and (b) MgO substrates with an intervening LSC layer.

PZT films deposited on [100]-oriented MgO substrates also exhibited high grain orientation, as shown by the x-ray diffraction pattern in Figure 3.6. The unit cell dimension established for the PZT film (c = 4.081 Å), using the d-values from the oriented pattern, is significantly larger than the unit cell dimension obtained for PZT films on SBN or $SrTiO_3$ substrates (Table 3.3). We believe that the films deposited on MgO are oriented along the [001] direction because the unit cell dimensions of PZT along the c-axis are larger (> 4.07 Å) and are closer to that of MgO (~ 4.21 Å). Further work is in progress to support this result.

Electrical measurements were carried out using Pt contact pads of either 0.00485 cm^2 or 0.0182 cm^2 area sputtered onto the film surface. Figure 3.7 shows the temperature dependence of the weak-field dielectric constant at 100 kHz for a PZT film on MgO/LSC. The ferroelectric phase transition, indicated by the dielectric maximum, is at 396 °C, somewhat higher than expected for a near-morphotropic PZT composition. The dielectric properties at lower frequencies are similar to that shown in Fig. 3.7 except for the appearance of excess boundary layer capacitance above 350°C due to the large conductivity in this region. Above 400 °C, the conductivity is nearly frequency-independent with an activation energy of 1.1 eV, a value considerably shallower than the 1.4 - 1.5 eV we have typically observed in good quality PZT ceramics. This suggests that the film stoichiometry is not yet as good as it could be.

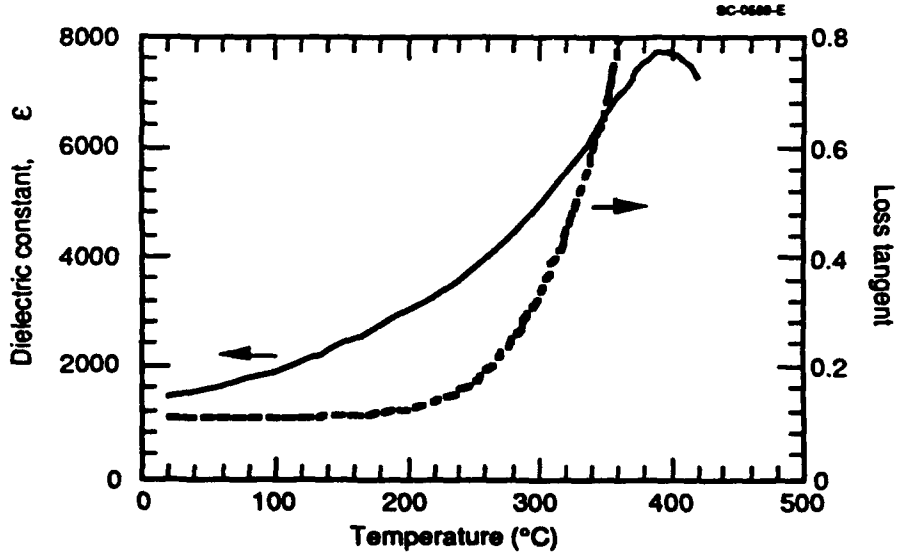

Figure 3.7 -- Temperature dependence of the dielectric constant and tan δ at 100 kHz for a PZT film on MgO/LSC.

Figure 3.8(a) shows the P-E hysteresis of the same PZT thin film measured at 23°C at a frequency of 25 Hz. The maximum applied field is ± 62 kV/cm, with a film coercive field E_c = 27 kV/cm. Above 80 kV/cm, the curve begins to distort in a manner suggesting non-linear space charge limited current injection consistent with the electronic Fermi level being far removed from a mid-gap position. The remanent polarization at zero bias was measured at 36 - 39 μcoulombs/cm^2, but because of the aforementioned space charge limited currents, these values may overestimate the true remanent polarization by up to 30%. Figure 3.8(b) shows the hysteresis loop for a PZT film on MgO/LSC after 5.5 x 10^7 cycles, with the vertical (polarization) scale expanded by a factor of two for clarity. P_r has reduced to 19.0 μcoulombs/cm^2 with only a slight increase in E_c to 29 kV/cm. The fatigue behavior of the remanent polarization with repeated hysteresis cycles is shown in Figure 3.9, where it is seen that P_r remains essentially constant above 6 x 10^6 cycles with no evidence of any further fatigue up to 2.6 x 10^8 cycles. In light of the discussion above, it is uncertain how much of this fatigue behavior may be attributed to an actual decline of P_r. Nevertheless, the limiting value of 18.5 μcoulombs/cm^2, which remains essentially constant even for field maxima above 100 kV/cm, is extremely good.

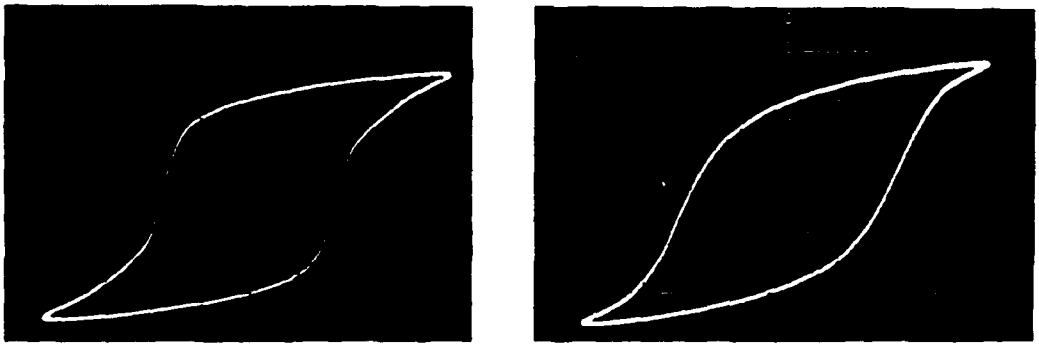

(a) After 500 cycles. f = 25 Hz, P_r = 36.5 μcoul/cm^2.

(b) After 5.5 x10^7 cycles. P_r = 19 μcoul/cm^2. Vertical scale (2x).

Figure 3.8 -- Polarization vs electric field for a PZT film deposited on MgO.

Table 3.4 summarizes the room-temperature properties of the sol-gel PZT thin films grown on MgO, SBN:60 and $SrTiO_3$ substrates with intervening LSC contact layers. PZT films grown on the latter two substrates showed superior high-field behavior with essentially no evidence of space charge current injection or film breakdown for electric fields up to 130 kV/cm.

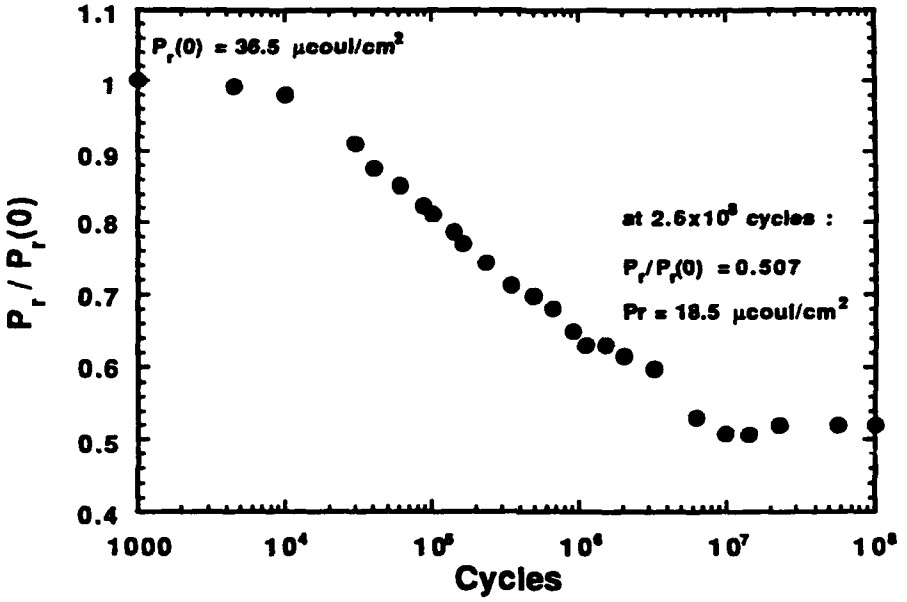

Figure 3.9 -- Electrical fatigue for a PZT film on MgO/LSC.

Table 3.4
Properties of PZT Films Grown on SBN, $SrTiO_3$ and MgO Substrates

Substrate	ε	P_3 (µcoul/cm²)		E_c (kV/cm)
		as measured	after $2x10^8$ cycles	
MgO	1390	36.5	19.0	27
SBN:60	1830	23.0	---	32
$SrTiO_3$	1100	19.0	---	38

3.2.2 Growth of $BaTiO_3$ Films

It is interesting to note that $BaTiO_3$ has an excellent lattice match with tungsten bronze SBN:60, SBN:50, and other important ferroelectric materials. The lattice mismatch with these substrates in the {001} direction is less than 0.5% and this allowed us to grow $BaTiO_3$ films with minimum strain. $BaTiO_3$ films have been grown by the same sputtering technique developed for other tungsten bronze films. For this growth, we use a single target containing $BaTiO_3$ with suitable dopant or dopants (to induce strong photorefractive effects). The growth conditions used for $BaTiO_3$ depositions are as follows:

Target - Substrate Distance:	5-6 cm
Input Power Density:	2.3 to 2.8 W/cm^2
Gas Mixture:	Ar:O_2 (50:50)
Substrate temperature :	~300 °C
Annealing Temperature:	600-800 °C

The degree of grain-orientation obtained in this system depends on the substrate temperature during the film deposition. As shown in Figure 3.10(a), when the deposition was made at substrate temperatures below 300°C, the films are essentially polycrystalline. However, when the substrate temperature was kept over 400°C during the deposition, the films are highly crystalline and they are oriented along the {100} direction. This is clearly shown in in Fig. 3.10(b) by the fact that only the [100] and [200]-oriented $BaTiO_3$ peaks are observed when deposited on [001] oriented SBN:50 or SBN:60 substrates. In both these cases, the films were post annealed at 700°C after the deposition was terminated.

To use these $BaTiO_3$ films for photorefractive applications, one needs fast response and high coupling in the desired spectral range. For this reason, these films have been doped with either Fe^{3+} or Ce^{3+} and after such doping the films are highly photorefractive. However, the distribution of dopants within these films is not uniform. Consequently, in our future growth experiments, we plan deposit the doping material as discrete layers within the $BaTiO_3$ film.

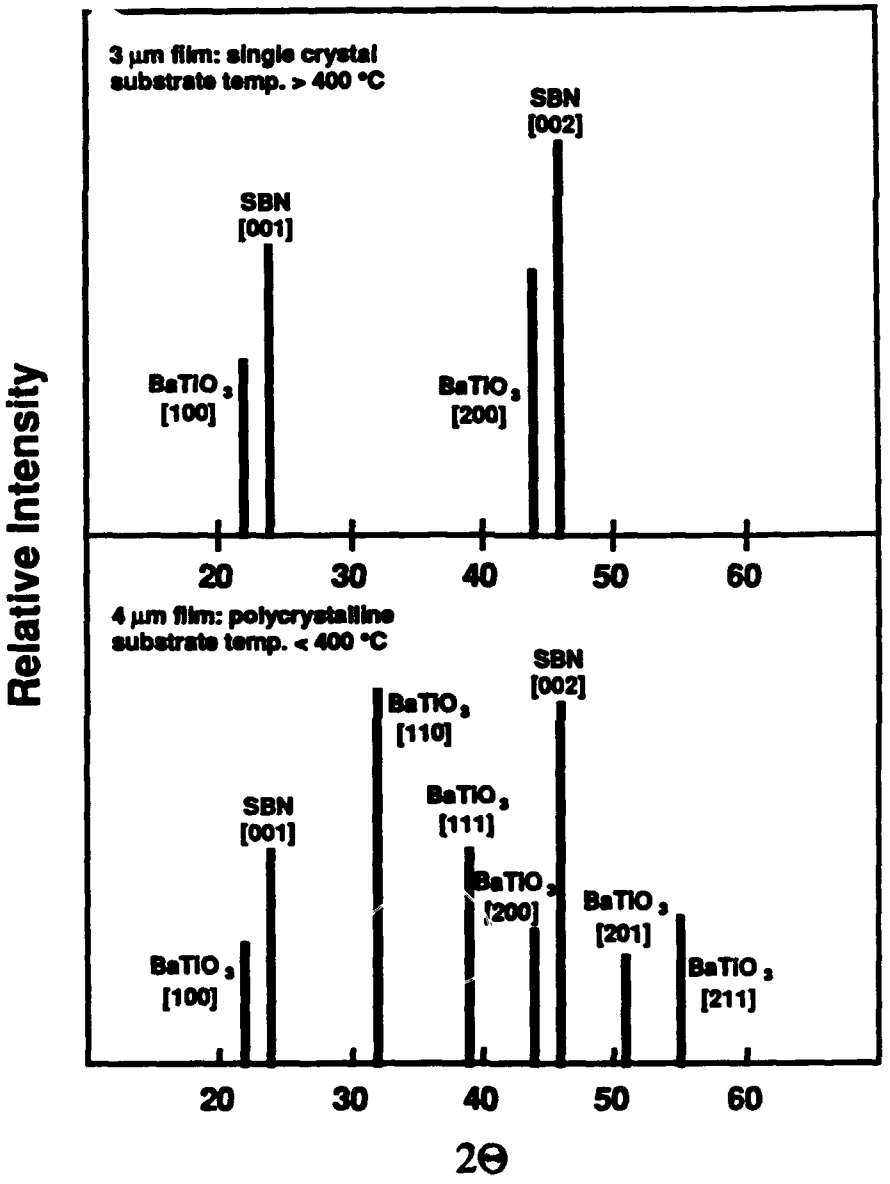

Figure 3.10 – X-ray diffraction pattern for $BaTiO_3$ films deposited on SBN substrates.

At present, efforts are underway to measure the temperature dependence of the dielectric properties for these films. The room temperature properties for $BaTiO_3$ films are as follows:

(a) $\varepsilon = 3000$

(b) $P_r = \sim 15\ \mu c/cm^2$

(c) $r_{ij} = >600 \times 10^{-12}\ m/V$

These are excellent values for thin film material, but we expect they will be significantly better by achieving a higher degree of grain-orientation.

This is the first time photorefractive $BaTiO_3$ films have been grown on SBN substrates for these types of applications and we expect that by controlling their photorefractive response, they will have great potential for various applications. Currently, we are optimizing the quality and photorefractive properties of both PZT and $BaTiO_3$ films and based on these investigations, the necessary changes in the film properties and quality will be made.

4.0 FUTURE PLANNED WORK

4.1 Multilayer SLM Concepts: Film Development

At UCSD, SLM designs are being formulated based on Professor Sing Lee's multilayer concepts which overcome the difficulties associated with Fabry-Perot designs in bulk ferroelectric crystal implementations. This concept shows that an optimum modulation response can be obtained for multilayer stack containing approximately 20 layers of $\lambda/4$ thickness (as shown in Fig. 4.1). Efforts are underway the Rockwell International Science Center to fabricate multilayer stacks consisting of 20 alternating layers of PLZT and SBN using both sputtering and sol-gel techniques. In our initial work, we plan to concentrate only on Si substrates.

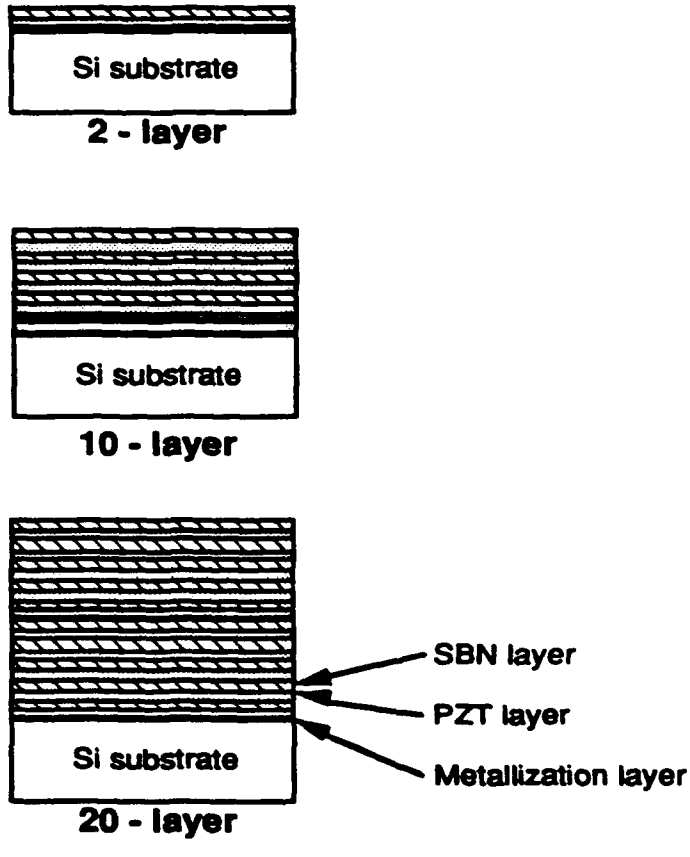

Figure 4.1 – Multilayer PLZT and SBN stacks: (a) two layers, (b) 10 layers and (c) 20 layers.

4.2 Photorefractive Films

The photorefractive films are being optimized with respect to the channel waveguides and holographically controlled switching devices. These applications require films that possess suitable optical quality and appropriate photorefractive characteristics. Since the film quality has been sufficiently good to test these concepts, we studied these films by a two wave mixing technique and found that the photorefractive properties are not adequate due to nonuniform distribution of dopants in the films. These films were grown using a single target which contained both the film and dopant materials. Differences in sputter rates between the two materials caused severe problems in controlling the distribution of dopants within the films. In order to achieve more uniform doping throughout the films, we are currently depositing the dopant from a second target as completely separate layers. Using this scheme, the doping concentration is controlled by varying the thickness and number of doping layers. We expect that the photorefractive properties in these new films should be more uniform and should allow us to characterize their role for various applications. The quality of these films also depends on the SBN substrate and for this reason we are spending significant effort to achieve high quality substrates polished to an excellent optical finish.

APPENDIX 5.1

Grain-Oriented Ferroelectric PZT Thin Films on Lattice-Matched Substrates

Mat. Res. Bull., Vol. 28, pp. 719-727, 1993. Printed in the USA.
0025-5408/93 $6.00 + .00 Copyright (c) 1993 Pergamon Press Ltd.

GRAIN ORIENTED FERROELECTRIC PZT THIN FILMS ON LATTICE-MATCHED SUBSTRATES

R. R. Neurgaonkar, I. S. Santha, J. R. Oliver, J. G. Nelson,
J. T. Cheung and P.E.D. Morgan
Rockwell International Science Center
Thousand Oaks, CA 91360

and

K. R. Udayakumar
Pennsylvania State University
University Park, PA 16802

(Received September 29, 1992; Communicated by W.B. White)

ABSTRACT

The sol-gel technique has been used to produce highly grain-oriented perovskite PZT thin films on lattice-matched SBN:60, $SrTiO_3$ and MgO substrates. These films were deposited on both $La_{0.5}Sr_{0.5}CoO_3$ (LSC) laser ablated-coated and uncoated substrates and annealed in the range of 630-675°C in an air or oxygen atmosphere. In all cases the PZT thin films were highly crystalline and oriented, with dielectric constants higher than 1100. The measured remanent polarization in these films exceeded 18 μcoul/cm^2 indicating the potential for strong electro-optic and piezoelectric effects.

MATERIALS INDEX: thin films, ferroelectric materials, sol-gels

Introduction

Ferroelectric thin films that are highly grain-oriented are crucial elements in various electro-optic and photorefractive device concepts such as optical modulators and holographic switches. Fabrication of such films has proven difficult, particularly when precise compositional control is needed. We have grown various tungsten bronze and

perovskite ferroelectric films on SBN substrates using liquid phase epitaxy (LPE), sputtering and sol-gel techniques (1-8). In the first two cases film composition is hard to control, while in the sol-gel process, obtaining grain-orientation is difficult.

In this paper, we report the successful growth of highly grain-oriented PZT thin films on various lattice-matched substrates (SBN:60, $SrTiO_3$ and MgO) by the sol-gel technique. We were encouraged to try this technique by the success of Hirano et al. (9) in the growth of grain-oriented $LiNbO_3$ films on sapphire (Al_2O_3). While single crystal PLZT films have been produced on lattice-matched $SrTiO_3$ by the rf sputtering technique (10), this is the first demonstration of sol-gel growth to produce highly crystalline ferroelectric PZT films on tungsten bronze SBN, $SrTiO_3$ and MgO substrates. In addition interesting results were obtained when using an electrical conducting buffer layer of $La_{0.5}Sr_{0.5}CoO_3$ (LSC). Highly electrically conducting perovskites have been known for many years (11), with LSC particularly known to exhibit outstanding high electrical conductivity (12, 13) and lattice parameters (14) suitable for matching to many ferroelectric (and other perovskites) materials. Thus epitaxial metallic electrode/insulating interfaces can be achieved with minimal stress which then may be anticipated to demonstrate very good fatigue properties.

Experimental Procedure

1. Preparation of Stock Solution

The procedure followed for preparation of sol-gel solutions has been outlined in detail by Udayakumar et al. (15,16). Lead acetate trihydrate was dissolved in heated 2-methoxyethanol at a 1:26 molar ratio in a three-neck reaction flask. The solution was then heated to above 100°C and maintained at the same temperature for 1-2 hours to remove the water of hydration. The dehydrated solution was cooled to room temperature before the required amount of titanium iso-propoxide and Zirconium-n-propoxide were added sequentially under a dry argon atmosphere. The solution was then refluxed for several hours to promote complexation. Thereupon, the solution was heated until the temperature of the condensing vapor reached that of pure 2-methoxyethanol. The final concentration of the solution was adjusted to 1 M by either the removal or addition of 2-methoxyethanol. The 1M complex alkoxide solution was stored in a dry box.

As discussed by Shimuzi et al. (15), a thin- film precursor solution was prepared by combining equal volumes of the stock solution and 2-methoxyethanol. Hydrolysis was realized from the moisture in the ambient. Thin films fabricated from solutions prepared by a similar procedure delineated above have reproducibly shown excellent electrical characteristics (17).

2. Thin Film Growth

The substrate structure employed in this study consisted of 500Å Ti / 1000Å Pt and $La_{0.5}Sr_{0.5}CoO_3$ (LSC) as a buffer layer applied by laser ablation (8,18) on lattice-matched SBN:60, MgO and $SrTiO_3$ substrates. Thin films were fabricated on the substrate by spin coating at 3000-5000 rpm for 25 seconds. Following the procedure of Dey and Zuleeg (19), the films were pyrolyzed in air above 200°C, and the cycle was repeated until the desired thickness was obtained. In the present work, film thicknesses were in the range of 0.5 to 2.0 μm to establish the ferroelectric and structural properties.

The film-coated samples were annealed at elevated temperatures in air or oxygen for a period of 2 to 3 hours. In the annealing process, the films were first held at 400°C for 30 minutes to ensure the complete pyrolysis of the organic with a heating rate of 10°C/min., and 5°C/min thereupon to the final annealing temperature (630-675°C). Since SBN substrates are ferroelectric at room temperature, films grown on SBN were cooled slowly through the phase transition temperature (78°C) to avoid cracking.

3. Thin Film Characterization

The phase purity and grain-orientation of the films were characterized by various x-ray diffraction techniques. The chemical composition of the films was determined by scanning electron microscopy. For ferroelectric measurements, platinum surface electrodes were used. The relative dielectric constant and dielectric loss tangent of the films were measured as a function of temperature and frequency using a multifrequency LCR meter (4274A, Hewlett Packard Co.). The polarization- field (P-E) hysteresis loop and fatigue were measured using a modified Sawyer-Tower circuit at 23°C .

Results and Discussion

Table 1 summarizes growth conditions for the PZT films and the results of each growth in terms of film thickness and degree of orientation. The most extensive set of growth experiments were carried out on SBN substrates. These included two different orientations with no buffer layer and conducting LSC buffer layer. The conducting buffer layer allows direct measurements of the ferroelectric properties of the PZT films.

TABLE 1
Growth Conditions for PZT Films

Substrate	Annealing Temp (°C)	Thickness (μm)	Film Orientation	Unit Cell (Å)
SBN Substrate				
(001) No Coating	640-675	0.5 to 1.5	(100) oriented	4.015
(001) LSC-Coating	620-640	0.5 to 1.0	(100) oriented	4.021
(100) No Coating	640-675	0.5 to 1.0	polycrystalline	---
$SrTiO_3$ Substrate				
(100) No Coating	620-635	0.5 to 1.0	(100) oriented	3.992
(100) LSC Coating	620-635	0.5 to 1.2	(100) oriented	3.995
MgO Substrate				
(100) No Coating	640-650	0.5 to 1.0	partially oriented	4.081
(100) LSC Coating	640-650	0.5 to 1.0	(100) oriented	4.081

As shown by the x-ray diffraction patterns in Figure 1, the PZT films deposited on (001) SBN:60 substrates are highly oriented along the (100) direction of the perovskite structure because of the close lattice match between (100) PZT and (001) SBN:60. This is the first time the sol-gel process has been successfully used to grow highly grain-oriented PZT films on SBN. Since the refractive index difference between PZT

and SBN:60 is large ($\Delta n \sim 0.218$), this structure could have significant impact on photorefractive and electro-optic applications. We are currently adjusting the film composition to improve the lattice match with SBN:60, which will lead to lower strain and lower defect oriented films. In contrast, PZT films grown on (100)-oriented SBN:60 substrates are typically lattice-mismatched and therefore the films are polycrystalline with no preferred orientation.

Also shown in Figure 1 is the diffraction pattern for PZT grown on SBN/LSC. The LSC buffer layer grows as a highly oriented cubic perovskite on SBN:60 with a lattice constant slightly lower than the c-axis value for SBN. For this reason, the subsequent PZT layer also achieves good grain orientation.

Figure 2 shows the x-ray diffraction patterns for grain-oriented PZT films on LSC coated $SrTiO_3$ and MgO. Since the film, substrate and buffer layers are all perovskite, we expected that the crystallinity of the PZT films on $SrTiO_3$/LSC should be good. It has been reported that single crystal PZT films have been grown by *rf* sputtering on (100)-oriented $SrTiO_3$ substrates for optical applications (10), but this is the first instance of sol-gel growth of such films. Efforts are under way to study the film quality for optical applications using (110) and (111)-oriented $SrTiO_3$ substrates.

PZT films deposited on (100)-oriented MgO substrates also indicated high grain orientation, as shown by the x-ray diffraction pattern in Figure 3. The unit cell dimension established for the PZT film ($c = 4.081$Å), using the d-values for the oriented pattern, is significantly larger than the unit cell dimension obtained for PZT films on SBN or $SrTiO_3$ substrates (Table 1). We believe that the films deposited on MgO are oriented along the (001) direction because the unit cell dimensions of PZT along the c-axis are larger (> 4.07Å) and are close to that of MgO (~ 4.21Å). Further work is in progress to support this result.

Electrical measurements were carried out using Pt contact pads of either 0.00485 cm^2 or 0.0182 cm^2 area sputtered onto the film surface. Figure 3 shows the temperature dependence of the weak-field dielectric constant at 100 kHz for a PZT film on MgO/LSC. The ferroelectric phase transition, indicated by the dielectric maximum, is at 396°C, somewhat higher than expected for a near-morphotropic PZT composition. The dielectric properties at lower frequencies are similar to that shown in Figure 3 except for the appearance of excess boundary layer capacitance above 350°C due to the large conductivity in this region. Above 400°C, the conductivity is nearly frequency-independent with an activation energy of 1.1 eV, a value considerably shallower than the 1.4 - 1.5 eV we have typically observed in good quality PZT ceramics. This suggests that the film stoichiometry is not yet as good as it could be.

Figure 4(a) shows the P-E hysteresis of the same PZT thin film measured at 23°C at a frequency of 25 Hz. The maximum applied field is ± 62 kV/cm, with a film coercive field $E_c = 27$ kV/cm. Above 80 kV/cm, the curve begins to distort in a manner suggesting non-linear space charge limited current injection consistent with the electronic Fermi level being far removed from a mid-gap position. The remanent polarization at zero bias was measured at 36 - 39 μcoulombs/cm^2, but because of the aforementioned space charge limited currents, these values may overestimate the true remanent polarization by up to 30%. Figure 4(b) shows the hysteresis loop for a PZT film on MgO/LSC after 5.5×10^7 cycles, with the vertical (polarization) scale expanded by a factor of two for clarity. P_r has reduced to 19.0 μcoulombs/cm^2 with only a slight

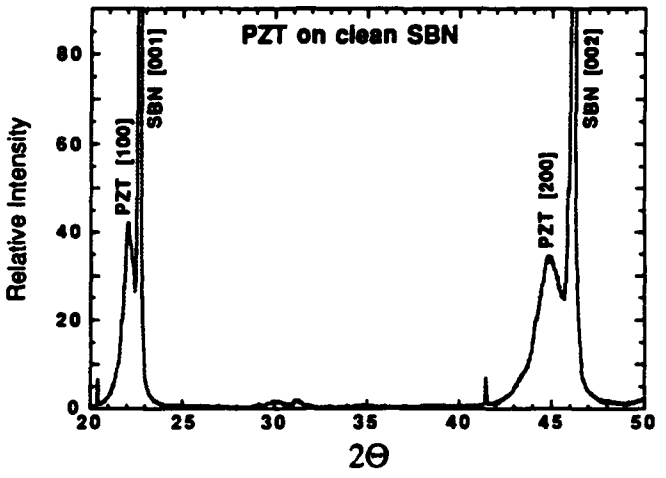

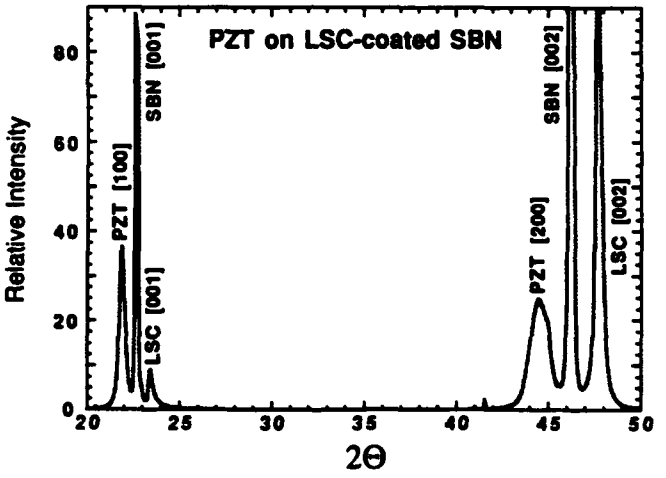

Figure 1 - X-ray diffraction pattern of PZT films on SBN substrates.

increase in E_c to 29 kV/cm. The fatigue behavior of the remanent polarization with repeated hysteresis cycles is shown in Figure 5, where it is seen that P_r remains essentially constant above 6 x 10^6 cycles with no evidence of any further fatigue up to 2.6 x 10^8 cycles. In light of the discussion above, it is uncertain how much of this fatigue behavior may be attributed to an actual decline of P_r. Nevertheless, the limiting value of 18.5 μcoulombs/cm^2, which remains essentially constant even for field maxima above 100 kV/cm, is extremely good.

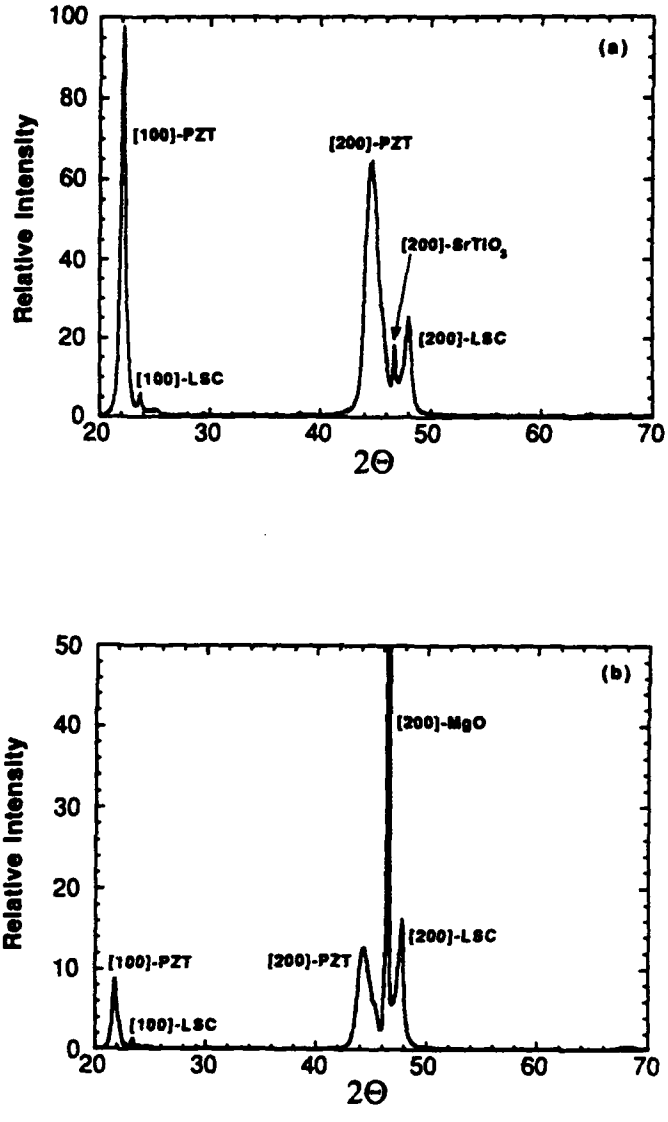

Figure 2 - X-ray diffraction patterns for PZT films on (a) $SrTiO_3$ and (b) MgO substrates with intervening LSC layer.

Table 2 summarizes the room-temperature properties of the sol-gel PZT thin films grown on MgO, SBN:60 and $SrTiO_3$ substrates with intervening LSC contact layers. PZT films grown on the latter two substrates showed superior high-field behavior with essentially no evidence of space charge current injection or film breakdown for electric fields up to 130 kV/cm.

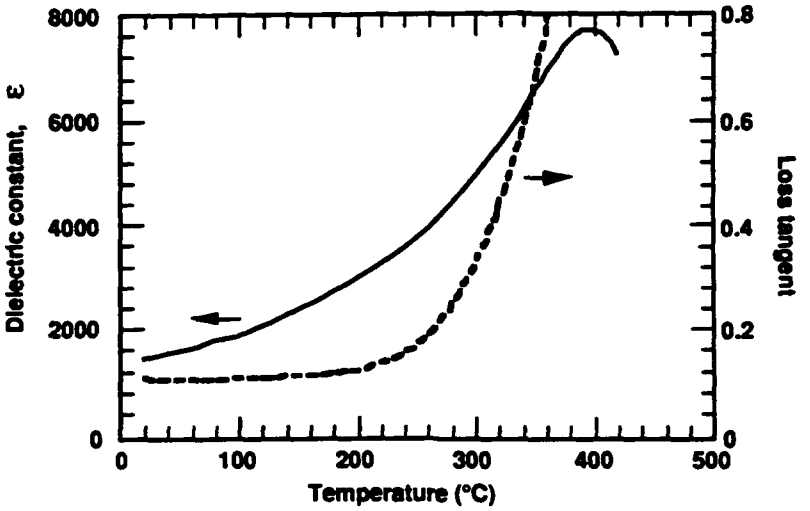

Figure 3 - Temperature dependence of the dielectric constant and Tan δ at 100 kHz for a PZT Film on MgO/LSC

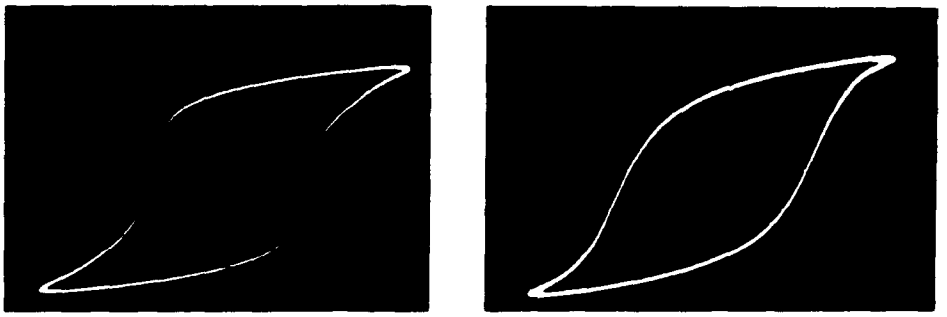

(a) After 500 cycles. f = 25 Hz, P_r = 36.5 μcoul/cm^2.

(b) After 5.5 x10^7 cycles. P_r = 19 μcoul/cm^2. Vertical scale expanded 2X.

Figure 4 - Polarization vs electric field for a PZT film deposited on MgO.

TABLE 2
Properties of PZT Films Grown on SBN, $SrTiO_3$ and MgO Substrates

Substrate	ε	P_3 (μcoul/cm²) as measured	P_3 (μcoul/cm²) after $2x10^8$ cycles	E_c (kV/cm)
MgO	1390	36.5	19.0	27
SBN:60	1830	23.0	----	32
$SrTiO_3$	1100	19.0	----	38

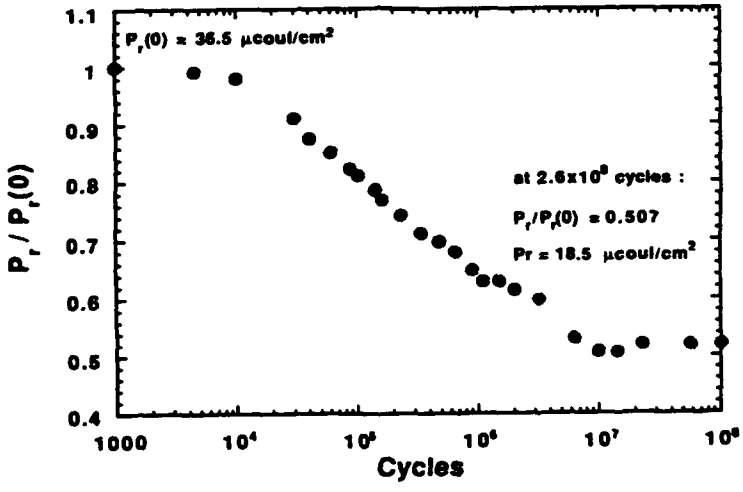

Figure 5 - Electrical fatigue for a PZT film on MgO/LSC.

Conclusions

We have presented our preliminary work on the growth of highly grain-oriented PZT films using the sol-gel technique. These films show high remanent polarization and high dielectric constants, indicating that the electro-optic and piezoelectric properties should be proportionately large. These properties can be increased further by adjusting the film composition and stoichiometry . The successful development of these films will open up a variety of optical applications using the electro-optic effect (modulators and waveguides) and the photorefractive effect (switches, image processing, pattern recognition and neural network).

Acknowledgments

This work was supported by DARPA (Contract No F49620-90-C-0084) and by Rockwell International Independent Research and Development (IR&D). The authors are grateful for discussions on this work with Professor L. E. Cross of the Pennsylvania State University.

References

1. R. R. Neurgaonkar, M. H. Kalisher, E. J. Staples and T. C. Lim, Appl. Phys. Lett. 35 (8), 606 (1979).
2. R. R. Neurgaonkar, T. C. Lim, E. J. Staples and L. E. Cross, Ferroelectrics 27, 62 (1980).
3. R. R. Neurgaonkar and E. J. Staples, J. Cryst. Growth 27, 352 (1981).
4. R. R. Neurgaonkar and E. T. Wu, Mat. Res. Bull. 22 (8), 1095 (1986).
5. R. R. Neurgaonkar, J. R. Oliver and L. E. Cross, Mat. Lett. 6 (5-6), 152 (1988).
6. R. R. Neurgaonkar, I. Santha, J. R. Oliver, E. T. Wu and L. E. Cross, J. Mat. Science 25, 2053 (1990).
7. R. R. Neurgaonkar, I. S. Santha and J. R. Oliver, submitted to Mat. Res. Bull.
8. J. T. Cheung, P. E. D. Morgan and R. R. Neurgaonkar, private communication.
9. S. Hirano, T. Yogo, K. Kikuta, K. Kals, W. Sakamoto and S. Ogasahara, Ceram. Transaction 25, 19 (1991).
10. Y. Higuma, K. Tanaka, T. Nakagawa, T. Kariya and Y. Hamakawa, (Jap) J. Appl. Phys. 16 (9), 1707 (1977).
11. P. E. D. Morgan, Proc. Workshop on High Temperature Solid Oxide Fuel Cells, H. S. Isaacs, S. Srinivasan and I. L. Harry, Eds., BNL 50765, 54 (1977).
12. G. H. Jonker and J. H. Van Santen, Physica 19, 120 (1953).
13. P. E. D. Morgan, J. Am. Ceram. Soc. 58, 349 (1975).
14. P. M. Raccah and J. Goodenough, J. Appl. Phys. 39, 1209 (1968).
15. Y. Shimizu, K. R. Udayakumar and L. E. Cross, J. Am. Ceram. Soc. 74 (12), 3023 (1991).
16. K. R. Udayakumar, J. Chen, S. B. Krupanidhi and L. E. Cross, Proc. of 7th IEEE, ISAF, 741 (1990).
17. K.R. Udayakumar, S.F. Bart, A.F. Flint, J. Chen, L. Tavrow, L.E. Cross, R. Brook and D.J. Ehrlich, Proc. 4th IEEE Workshop on Microelectro Mechanical Systems, 109 (1991).
18. P. E. D. Morgan, 14th University Conf., "Processing of Crystalline Ceramics," Materials Science Research 11, 67, Eds, H. Pamour III, R. F. Davis, T. M. Hare, Plenum Press (1978).
19. S. K. Dey and R. Zuleeg, Ferroelectrics 108, 37 (1990).

APPENDIX 5.2

Growth of Grain-Oriented Tungsten Bronze SBN Films on Si

GROWTH OF GRAIN-ORIENTED TUNGSTEN BRONZE SBN FILMS ON Si

R.R. Neurgaonkar, I.S. Santha and J.R. Oliver
Rockwell International Science Center
Thousand Oaks, CA 91360

(Received May 28, 1991; Communicated by W.B. White)

ABSTRACT

This paper reports preliminary results on the growth of grain-oriented tungsten bronze Ce-doped $Sr_{1-x}Ba_xNb_2O_6$ (SBN) thin films on (100)-oriented Si substrates. Grain orientation was maintained in these films up to 4 μm thickness using high oxygen pressure annealing up to 700°C. The films are smooth and have excellent surface quality. The temperature dependence of the dielectric constant indicates the phase transition is near 30°C, with a dielectric constant of 1400 at room temperature. The spontaneous polarization for these films is 1.3 μcoul/cm² at room temperature and 6.5 μcoul/cm² at -125°C.

MATERIALS INDEX: SBN, grain-orientation, polarization

INTRODUCTION

The integration of ferroelectric thin films with semiconductor substrates is important for optoelectronic applications. Progress has been made in developing deposition techniques; however, grain-orientation has proven to be difficult to achieve on semiconductor substrates. We report here the successful deposition of tungsten bronze (T.B.) SBN ferroelectric thin films on Si substrates in which good grain-orientation was obtained.

The T.B. SBN solid solution exists on the binary $SrNb_2O_6$-$BaNb_2O_6$ system with the highest electro-optic and piezoelectric coefficients for the $Sr_{0.75}Ba_{0.25}Nb_2O_6$ (SBN:75) composition (1-3). At Rockwell, we have been developing ferroelectric crystals in the tungsten bronze family for photorefractive and electro-optic applications since 1978 (4-10). Recently, we have focused our attention on developing single crystal and grain-oriented T.B. thin films for photorefractive, electro-optic and electronic memory applications. Earlier we had demonstrated the growth of single crystal SBN and SKN thin films on SBN:60 substrates by the LPE technique for SAW device applications (11,12). The growth of polycrystalline SBN films on glass and Si substrates has been reported recently by McKinzie et al (13-16), using the sol-gel process. The ferroelectric

properties that can be achieved in such films are greatly reduced from those found in single crystals of the same composition. For this reason, we are pursuing the magnetron sputtering technique for the growth of various tungsten bronze films to achieve good grain orientation on semiconducting substrates. This paper reports the results for SBN films grown on Si.

EXPERIMENTAL PROCEDURE

Ce^{3+}-doped ferroelectric tungsten bronze SBN thin films were sputtered using a single 3" target consisting of sintered BaO, SrO, CeO_2 and Nb_2O_5. Initial experiments indicated that the use of a stoichiometric target (SBN:75) produced nonferroelectric SBN films with an excess of Ba^{2+}. To maintain stoichiometry in the film, we incorporated 20% excess Sr^{2+} in the target to produce ferroelectric SBN films having a composition close to SBN:75. The final targets were prepared using ceramic sintering or hot-pressing; well-mixed powders were cold pressed and then sintered or hot-pressed at 1300°C.

The SBN thin films were deposited with an MRC rf sputtering instrument; the sputtering conditions are summarized in Table 1. (100)-oriented Si substrates of 10 × 10 × 1 mm were used for this study with platinum as an electrode on one surface. The substrate temperature was maintained below 300°C to avoid the oxidation of Si. The films were annealed in argon and then in oxygen below 700°C to achieve the desired tungsten bronze tetragonal structure (4mm).

X-ray diffraction was used to check the crystal structure and lattice constants of the films. The phase transition temperature, dielectric constant and spontaneous polarization were measured using standard ferroelectric measurement techniques (5,6).

RESULTS AND DISCUSSION

Since SBN:75 exhibits a large spontaneous polarization at room temperature ($P_3 > 24$ μcoul/cm²) and a large electro-optic coefficient ($r_{33} = 1400 \times 10^{-12}$ m/V), this composition is very promising for applications including spatial light modulators (SLM's), guided wave optics, photorefractive devices and electronic memories. SBN:75 has an excellent lattice-match with Si in one of the possible orientations ($a/\sqrt{2} = 3.901$Å). In the present work, we selected this orientation to fabricate grain-oriented SBN films on Si. A platinum electrode was sputtered on the growth surface with a thickness of less than 1000Å. The substrates were mounted on a heating block with a stainless steel mask of 0.2 mm thickness. Substrate temperature was monitored by a Pt-Pt Rh thermocouple inserted into the center of the substrate holder. The sputtering conditions are summarized in Table 1.

TABLE 1

Target-Substrate Distance:	5 cm
Sputtering Gas:	Ar:O_2
Substrate Temperature:	100-300°C
Deposition Rate:	10-15Å/min.
Annealing Temperature:	600-700°C

Figure 1 shows the x-ray diffraction patterns of SBN films grown on Si substrates for growth temperatures of 100° and 300°C, followed by annealing at 675°C. As shown in Figure 1a, excellent grain-orientation was achieved for films annealed above

600°C. Below this temperature, the films were essentially amorphous. We have also demonstrated the growth of grain-oriented perovskite PLZT and tungsten bronze PBN:60 and PSKNN thin films on Si substrates with good success (17,18), but in these cases the annealing temperature was near 600°C. Our current work indicates that grain orientation in these films strongly depends on the $Ar:O_2$ ratio during deposition as well as annealing. If the oxygen partial pressure is sufficiently low, Nb^{5+} converts to Nb^{4+} and this prevents the formation of the tungsten bronze phase. For this reason, we maintained a high oxygen pressure during annealing. Furthermore, we observed that the grain orientation is also very sensitive to the film thickness. Currently we have been successful in maintaining complete grain-orientation up to 3-4 μm with excellent film quality. Beyond this limit, mixed orientation films were observed with the (001)-oriented x-ray diffraction peaks being dominant. This thickness is sufficient for various optoelectronic applications, whereas for electronic memories, thicknesses in the range of 1000 to 3000Å are required.

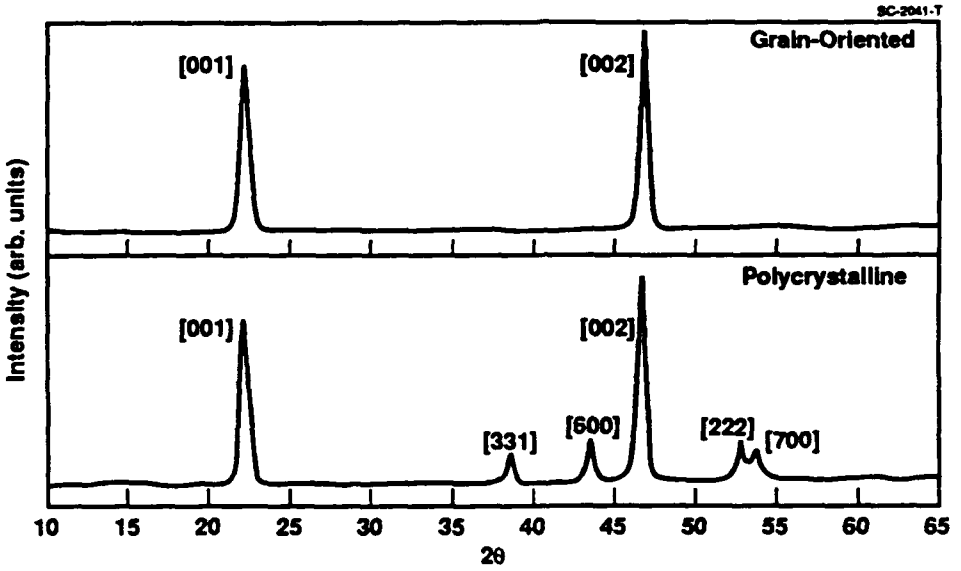

FIG. 1
X-ray diffraction patterns for SBN:75 films grown at (a) 300°C and (b) 100°C.

Lattice constant measurements on both (001)-oriented and polycrystalline SBN films show a = 12.456Å and c = 3.912Å indicating that the film composition is close to SBN:75. However, these results suggest that the films are still slightly Ba^{2+}-rich and can be adjusted to the desired composition by adjusting the Ba:Sr ratio in the target. The film surface and quality are quite adequate to make both ferroelectric and optical measurements, and the addition of Ce^{3+} did not degrade the film quality or change the growth conditions. This dopant was incorporated in the films to enhance their photorefractive properties; however, for linear electro-optical applications (e.g., modulators), such doping would not be utilized.

Figure 2 shows the temperature dependence of the weak-field dielectric constant at 10 kHz for 1.0 μm SBN film, using the substrate Pt metallization and an 0.018 cm^2 Pt surface contact as electrodes. The temperature of the dielectric maximum, T_C, varies with frequency from 27-42°C over a 100 Hz-100 kHz range, typical of a broadened relaxor phase transition. At room temperature the dielectric constant varies from 1430-1170 over the same frequency range. The corresponding room tempera-

ture dissipation factor is 0.022-0.340 with frequency, with the high loss value at 100 kHz resulting primarily from the series sheet resistance of the substrate metallization. Although this is a nominally SBN:75 film composition, the addition of Ce^{3+}, combined with a mild compressive stress on the film due to differing film/substrate thermal expansion coefficients and with potential film compositional nonuniformity, result in a broadened ferroelectric phase transition located well below the usual 50-54°C transition temperature for SBN:75. Nevertheless, the dielectric constant shows a very well-defined peak typical of an SBN ferroelectric, a feature not often found in many ferroelectric thin films.

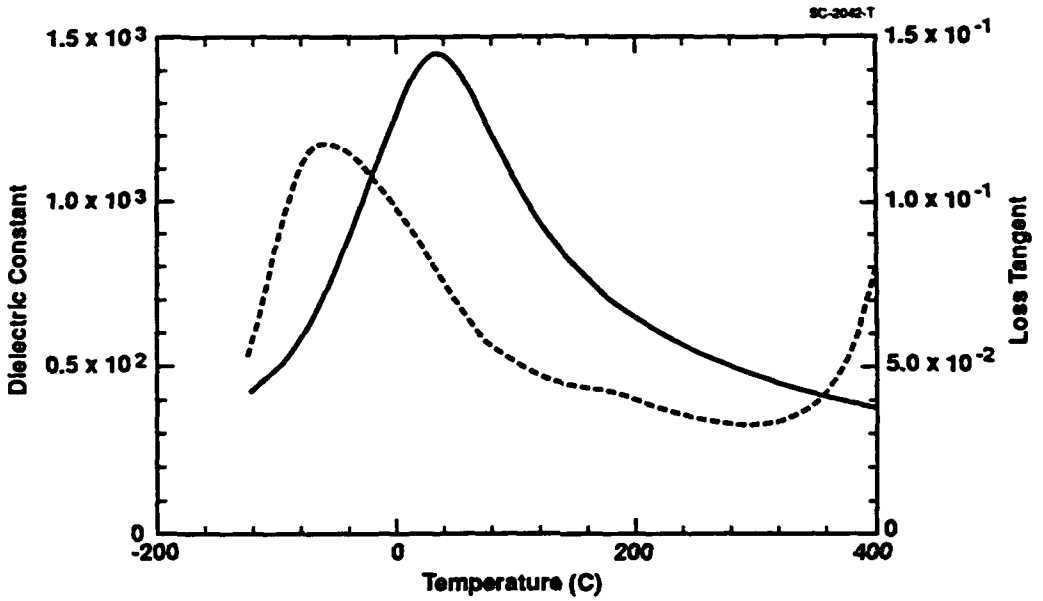

FIG. 2
Weak-field dielectric constant and tan δ at 10 kHz for an unpoled SBN:75 thin film.

Figure 3 shows the temperature dependence of the spontaneous polarization, P_S, measured by the integration of the short-circuit current density during warming at a constant rate of 3°C/min. Prior to measurement, the film was poled with an applied dc field of 40 kV/cm during cooldown from room temperature. The absence of an abrupt change in P_S near T_C again reflects the broadened distribution of phase transition temperatures in the film; this broadening results in the persistence of measurable polarization well above 100°C. Although P_S is only 1.3 μcoulombs/cm² at room temperature, it rises nearly linearly with decreasing temperature to a value of 6.5 μcoulombs/cm² at -125°C. These polarization values are among the highest reported thus far for SBN thin films.

The comparatively low spontaneous polarization at room temperature results in a slim-loop P vs E hysteresis, as shown in Figure 4(a). The reversible polarization, P_r, is 0.6 μcoulombs/cm², roughly one-half the value of P_S measured by thermal depolarization. However, at -95°C (Figure 4(b)), the loop begins to square out, with P_r = 4.6 μcoulombs/cm² and a coercive field E_C = 38 kV/cm. The reversible polarization agrees well with the measured P_S at -95°C (Figure 3); this correspondence holds true over most of the temperature range below 0°C.

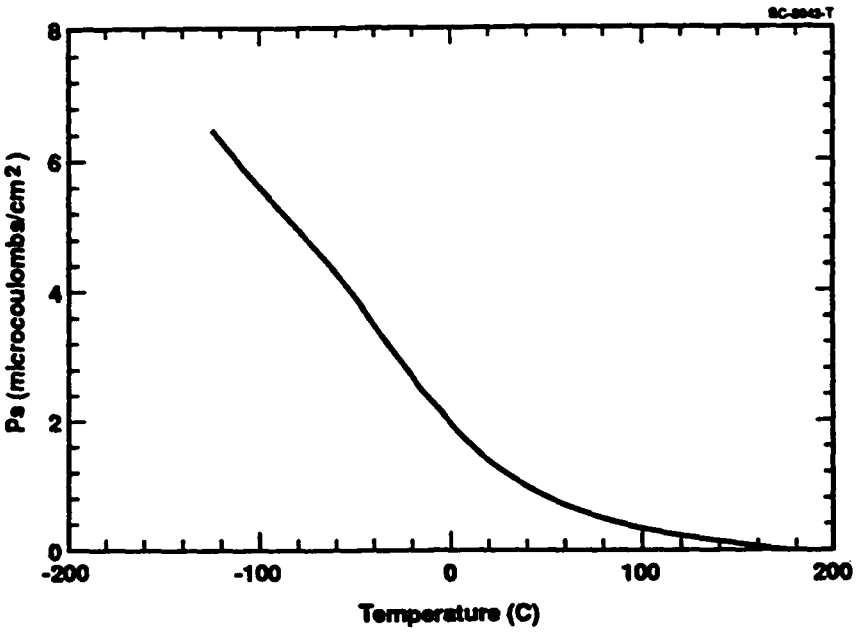

FIG. 3
Spontaneous polarization vs temperature for an SBN:75 thin film poled at 40 kV/cm.

FIG. 4
Polarization vs. electric field at 50 Hz for a 1.0 μm SBN:75 film: (a) at 23°C; (b) at -95°C. (Scales: horizontal - 50 kV/cm/div., vertical - 5 μcoul/cm²/div.)

No significant switching fatigue was observed in these films for up to 5×10^5 switching cycles at 50 Hz and temperatures at or below 23°C. What is noteworthy is that these SBN films can sustain electric fields of 150 kV/cm without breakdown, and still higher fields (> 200 kV/cm) at low temperatures.

CONCLUSIONS

We have presented x-ray and ferroelectric data for Ce^{3+}-doped SBN:60 thin films grown by sputtered deposition on Pt-metallized Si substrates. These films show good grain orientation with the polar c-axis normal to the film surface, and good dielectric and polarization properties. The present films, however, are limited by low spontaneous polarization at room temperature due to a broadened distribution of phase transition temperatures. This is due, in part, to possible excessive Ce^{3+} content in the films, combined with some degree of compositional nonuniformity. Nevertheless, the room temperature polarization of 1.3 μcoulombs/cm² ranks among the highest values measured in SBN films, and the dielectric constant is consistent with values found in high quality SBN single crystals. With continued improvement in film stoichiometry, compositional uniformity and grain orientation, these sputtered SBN thin films have the potential for effective use in a number of integrated electro-optical and photorefractive device applications.

ACKNOWLEDGMENTS

This work was supported by DARPA (Contract No. F49620-90-C-0084) and by the Office of Naval Research (Contract No. N00014-81-C-0463). The authors thank Prof. L. Eric Cross of the Pennsylvania State University for his useful discussions and suggestions during the course of this work.

REFERENCES

1. A.A. Ballman and H. Brown, J. Cryst. Growth 1, 321 (1967).
2. P.B. Lenzo, E.G. Spencer and A.A. Ballman, Appl. Phys. Lett. 11, 23 (1968).
3. R.R. Neurgaonkar and L.E. Cross, Mat. Res. Bull. 21, 893 (1986).
4. R.R. Neurgaonkar, M.H. Kalisher, T.C. Lim, E.J. Staples and K.L. Keester, Mat. Res. Bull. 15, 1305 (1980).
5. R.R. Neurgaonkar and W.K. Cory, J. Opt. Soc. Am. 3(B), 276 (1986).
6. R.R. Neurgaonkar, W.K. Cory, J.R. Oliver, M.D. Ewbank and W.F. Hall, J. Opt. Eng. 26(5), 392 (1987).
7. R.R. Neurgaonkar, W.K. Cory, J.R. Oliver, W.W. Clark III, G.L. Wood, M.J. Miller and E.J. Sharp, J. Cryst. Growth 84, 629 (1987).
8. R.R. Neurgaonkar, W.K. Cory, J.R. Oliver, E.J. Sharp, G.L. Wood, M.S. Miller, W.W. Clark III, and G.J. Salamo, Mat. Res. Bull. 23, 1459 (1988).
9. R.R. Neurgaonkar, W.K. Cory, J.R. Oliver, E.J. Sharp, M.J. Miller, W.W. Clark III, G.L. Wood and G.J. Salamo, Mat. Res. Bull. 24, 589 (1989).
10. R.R. Neurgaonkar, W.K. Cory, J.R. Oliver and L.E. Cross, Mat. Res. Bull. 24, 1025 (1989).
11. R.R. Neurgaonkar and E.T. Wu, Mat. Res. Bull. 22, 1095 (1987).
12. R.R. Neurgaonkar, J.R. Oliver and L.E. Cross, Mat. Lett. 6, 152 (1988).
13. R. Xu, Y.H. Xu, C.J. Chen, and J.D. Mackenzie, J. Mater. Res. 5(5), 916 (1990).
14. C.J. Chen, Y.H. Xu, R. Xu, and J.D. Mackenzie, J. Appl. Phys. 69, 1763 (1991).
15. Y.H. Xu, C.J. Chen, R. Xu, and J.D. Mackenzie, Phys. Rev. B., accepted for publication in July 1, 1991 issue.
16. C.J. Chen, Y.H. Xu, R. Xu, and J.D. Mackenzie, Electro-optics and Nonlinear Optic Materials, Ceramic Transaction 14, 211 (1990).
17. R.R. Neurgaonkar, I.S. Santha and J.R. Oliver, J. Mat. Science 25, 2053 (1990).
18. R.R. Neurgaonkar, I.S. Santha and J.R. Oliver, private communication.

APPENDIX 5.3

Epitaxial Growth of Highly Grain-Oriented PLZT Films on SBN Substrates by the Sputtering Technique

EPITAXIAL GROWTH OF HIGHLY GRAIN-ORIENTED PLZT FILMS ON SBN SUBSTRATES BY SPUTTERING TECHNIQUE

R. R. NEURGAONKAR, I. S. SANTHA AND J. R. OLIVER
ROCKWELL INTERNATIONAL SCIENCE CENTER
THOUSAND OAKS, CA 91360.

ABSTRACT

This paper reports the preliminary results of epitaxial growth highly grain-oriented PLZT thin films on tungsten bronze $Sr_{0.6}Ba_{0.4}Nb_2O_6$ (SBN:60) substrates by the rf sputtering technique. The films were deposited primarily with [001] SBN substrate orientation and temperatures > 500°C. These films exhibit excellent epitaxy with film orientation along the [100] direction. A multilayer approach has been proposed to improve film quality and properties.

INTRODUCTION

A lanthanum-modified lead-zirconate-titanate (PLZT) solid solution is a well known ferroelectric system. PLZT is transparent in the visible and near-infrared regions, has various electro-optic (1) and photochromic (2) activities, and promises excellent optoelectronic properties. There have been numerous concepts for its application in electronic and optoelectronic devices making use of these interesting properties e. g. in a nonvolatile FET memory with ferroelectric gates (3,4); optical switches (5); image storage (6); optical modulators (7); and, optical display devices (8). Considerable practical interest has been generated on a PLZT thin films for the purpose of reducing the device voltage, miniaturization and cost reduction of optoelectronic devices.

Quite recently, several attempts to prepare a PLZT films have been initiated using rf sputtering and electric beam evaporation (9-13) and some PLZT film possessing good ferroelectric properties have been obtained. However, from the viewpoint of applications in optical waveguide systems., the preparation of better thin films with high transparency is required. The most significant obstacle in obtaining good transparency and electro-optic properties is the difficulty in growing the perovskite structure with large grain size on suitable substrate materials during film deposition and heat treatment, since the grains increase absorption due to light scattering. We have conducted a series of experiments on the epitaxial growth of PLZT thin films on single crystal tungsten bronze $Sr_{0.6}Ba_{0.4}Nb_2O_6$ (SBN:60) substrates and have succeeded in growing PLZT films with good crystallinity. In this paper, the growth of these films, their structural properties and their applicability to electro-optic devices and in integrated optics are discussed.

EXPERIMENTAL PROCEDURE

The sputtering targets employed were a mixture of PLZT (7/60/40) and PbO. Approximately 5 mole% excess PbO was added in the targets to control Pb^{2+} concentration in the films. The targets were prepared using ceramic sintering or hot-pressing; well-mixed powders were cold pressed and then sintered or hot-pressed at 100°C after ball-milling. The Zr:Ti ratio was 60:40 and La^{3+} concentration was ~ 7% in these targets. The targets thus prepared showed no extra phases and were fabricated in 3" diameters to obtain uniform film deposition.

The PLZT thin films were deposited with an MRC rf sputtering instrument; the sputtering conditions are summarized in Table 1. SBN:60 crystals of dimensions 10 x 10 x 1 mm were cut in the [001] plane. Some of the substrates were polished to optical quality, etched with HF acid after polishing, or mechanochemically polished. The substrate temperature was maintained between

200-400°C during these film depositions.

Table 1

Growth of PLZT Thin Films on SBN Substrates

PLZT Film	Lattice-Match	As-Grown	Annealed Above 600°C	Lattice Constant	Remarks
(001)-oriented SBN:60 (substrate)					
≤ 400°C	0.40%	Weakly crystallized	Single crystal film	3.953Å	Excellent quality
≥ 550°C	0.40%	Well crystallized	Single crystal film	3.957Å	Excellent quality
Glass-Substrate					
≤ 400°C	—	Amorphous	<600°C pyrochlore >500°C perovskite	a = 3.961Å	Pyrochlore phase problem
≥ 550°C	—	Weakly crystallized pyrochlore	600°C perovskite (polycrystalline)	c = 4.121Å	
Lattice Constants:	SBN:60	a = 12.458Å,	c = 3.938Å		
	PLZT	a = 3.955Å,	c = 4.125Å		

RESULTS AND DISCUSSION

The epitaxial growth of PZT and PLZT has been subject of great interest for various applications, with film grwoht proving successful on various substrates (MgO, Si, SiO_2, Al_2O_3, Pt, glass, etc). However, the films obtained on these substrates are basically polycrystalline, with frequent occurrences of a pyrochlore phase. Recently, Higuma et al (14, 15) grew PLZT films on $SrTiO_3$ substrates and reported that the films were single crystal with excellent epitaxy. $SrTiO_3$ is cubic at room temperature with a lattice constant a = 3.905 Å, while PLZT can be either rhombohedral or tetragonal, depending upon the Zr:Ti ratio. The lattice constants for the tetragonal PLZT solid solution are a = 3.904 to 4.055 Å and c = 4.051 to 4.185 Å. Thus, one can adjust the film composition such that there is a good lattice match with the substrate. In the present work, we have employed tungsten brozne SBN:60 substrates which are tetragonal at room temperature with lattice constants a = 12.468 Å and c = 3.938 Å (16). The PLZT composition selected for epitaxial growth was PLZT (7/60/40) with lattice constants a = 3.955 Å and c= 4.125 Å. This composition has an excellent lattice match with SBN:60 in the following two orientations:

$[100]_{Film} = [001]_{Sub.}$ $[a_{film} = c_{sub}]$

$3 \times [001]_{film} = [100]_{Sub}$ $[3 \times c_{film} = a_{sub.}]$

As shown in Figure 1, 3 cm diameter, 7 cm long SBN:60 single crystals of optical quality are available and were used in these growths (17, 18). Two other tungsten bronze crystals having slightly bigger unit cells, SBN:50 and BSKNN-2, are also available for use as substrates.

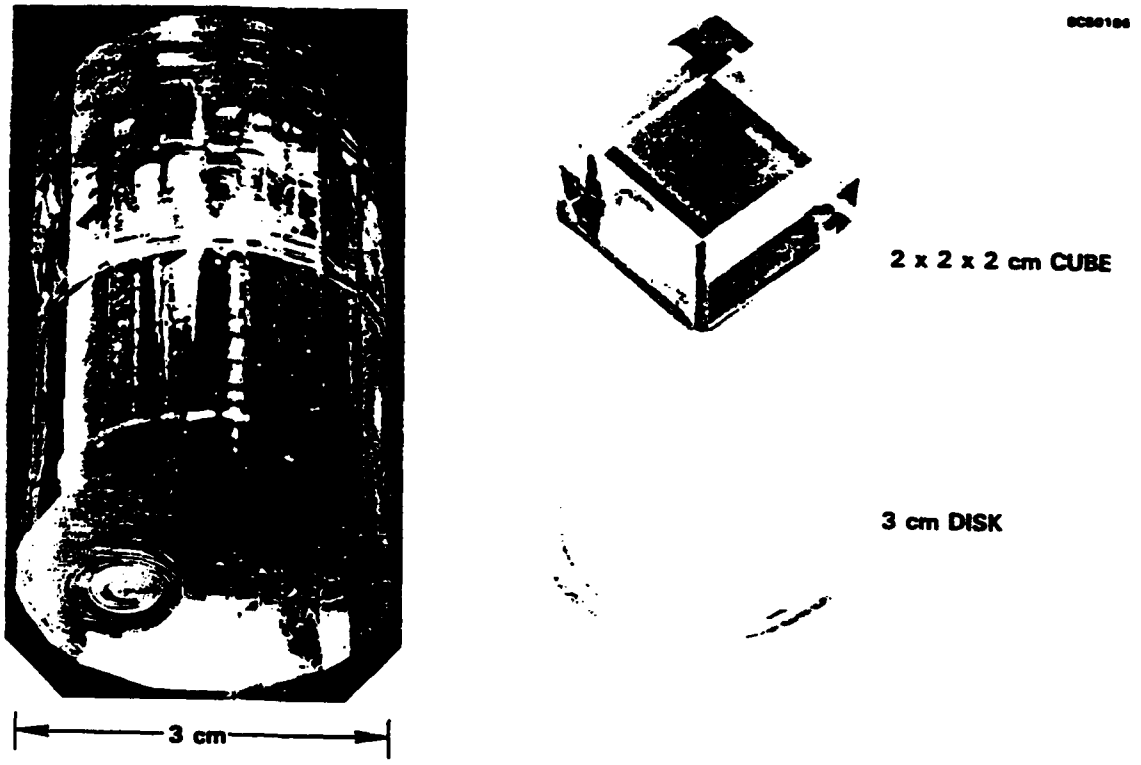

Figure 1: Tungsten Bronze SBN:60 Single Crystal and Product

PLZT thin films were deposited on [001] -oriented SBN:60 with substrate temperatures varied between 200 and 400°C. As summarized in table 1, all films were grown in an $Ar:O_2$ (argon:oxygen) atmosphere. The sputtering conditions were as follows:

- Target-Substrate Distance: 4 - 5 cm
- Input Power Density: 1.9 to 2.4 w/cm^2
- Gas Mixture: Ar:O_2 (50:50)
- Substrate Temperature: 200-400°C
- Deposition Rate: 50-100 A°/hr
- Annealing Temperature: 600-650°C.

Figure 2 shows x-ray diffraction pattern of PLZT thin films deposited on glass and SBN:60 substrates and annealed at 600°C. All of the tetragonal perovskite peaks of PLZT were observed when the film was deposited on glass, with the formation of the pyrochlore phase below 600°C. This result is consistent with work reported by various researchers, including our earlier work (5-15, 19). However, when the film was deposited on the [001]-oriented SBN:60 substrates, only the [100] and [200] diffractions peaks of the film were observed. This clearly shows that the PLZT film deposited on SBN are highly grain-orienetd with excellent epitaxy. We believe that this is the first time such perovskite films have been grown on tungsten bronze substrates.

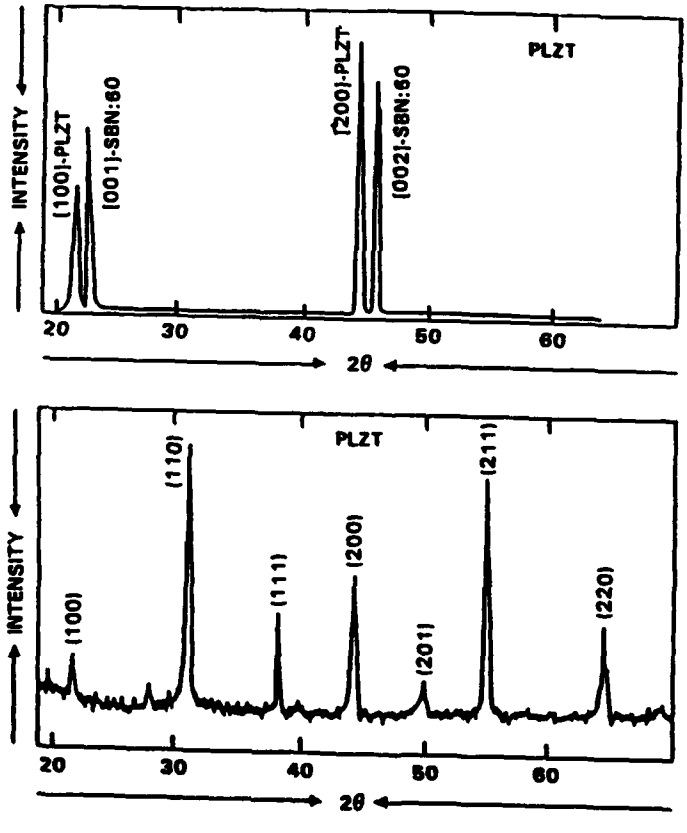

Figure 2: Perovskite PLZT Thin Films On T. B. SBN:60 Substrates.

The growth of PLZT films was investigated at various substrate temperatures and it was found that the films grown below 400°C were weakly crystallized and needed subsequent annealing above 500°C. However, films grown at substrate temperatures of 500°C or above were well crystallized, almost single crystal films. Furthermore, the use of SBN substrates completely suppressed the formation of the pyrochlore PLZT phase even at lower temperatures. On the other hand, PLZT films grown on other substrates such as glass, platinum, Al_2O_3 and quartz always exhibited a pyrochlore phase and required high temperature annealing to convert to the perovskite phase.

The occurrence of a pyrochlore phase is a subject of great interest in Pb2+-containing perovskites and it usually appears when the unit cell c/a ratio is below 1.06, as shown in Figure 3. Since c/a for $PbTiO_3$-$BiFeO_3$ is 1.17, one does not observe the pyrochlore phase on this system. On the other hand, the pyrochlore phase is found for all compositions in the $PbTiO_3$-$PbZn_{0.33}Nb_{0.67}O_3$ system. The latter is exceptionally important for electro-optic and piezoelectric applications because it exhibits both electro-optic and piezoelectric coefficients very large with a large spontaneous polarization.

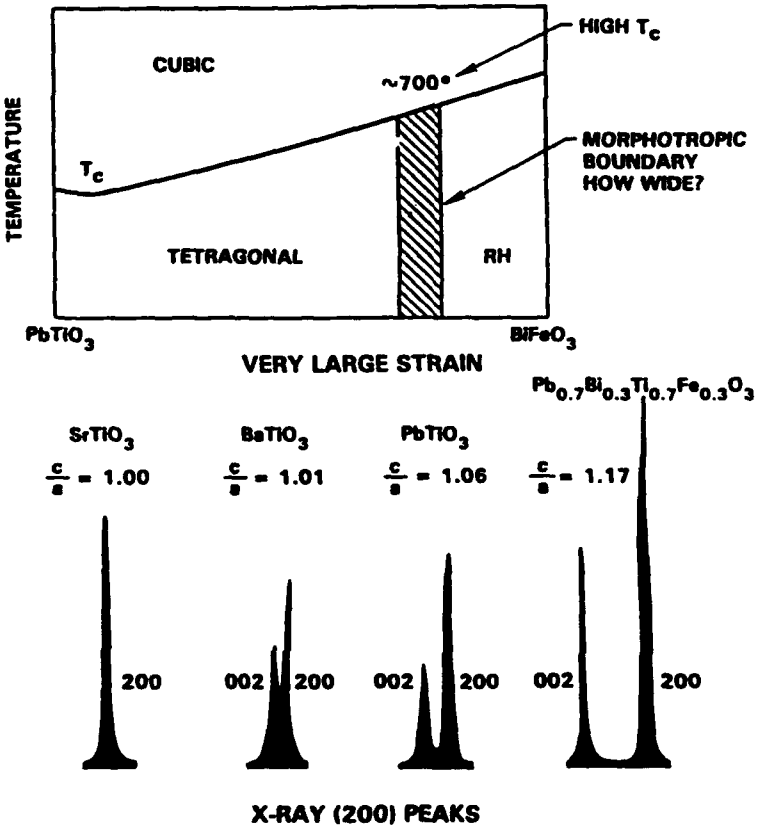

Figure 3: The Phase Diagram for Lead Titanate -Bismuth Ferrite System.

The lattice constant a is estimated to be 3.955 Å in the PLZT films, in close agreement with the ceramic value. Electron diffraction patterns need to be studied to ascertain the single and polar direction in these films. PLZT deposited on SBN:60 substrates are completely transparent in the visible, cutting off in the IR because of substrate absorption. According to work by Okuyama et al (15), PLZT films deposited on MgO and $SrTiO_3$ are transparent from visible to the near - IR. Optical measurement on their films suggest that the optical loss is about 6 db/cm, which is slightly higher than that of $LiTaO_3$ single crystals. However, the half-wave voltage is about one fourtieth of that for $LiNbO_3$ or $LiTaO_3$, and the reduction of the element size would compensate for the large loss factor. We suspect that this loss can be suppressed further by using well matched substrates such as SBN:60 or other lattice-matched tungsten bronze materials.

PLZT thin films grown in study will be used for two specific applications: 1) Guidedwave optical applications and 2) holographic data storage . In the first application, one needs undoped PLZT films to suppress completely the space charge field while in other case we need strong charge field to produce strong photorefractive effects for data storage applications. In order to increase this space charge field, we are incorporating specific dopants such as Fe^{2+}/Fe^{3+} and Ce^{3+}/Ce^{4+} in our PLZT films. The films are strongly photorefractive to use for data storage, but further work is necessary to improve the uniformity of these dopants in these films.

MULTILAYER THIN FILM CONCEPTS

Since the growth of highly grain-oriented PLZT thin films on SBN has been successful, it opens up various ways one can employ these films for optical applications. If the optical quality or optical loss remains a problem for device consideration, a multilayer approach may be appropriate for these films. Since tungsten bronze $Pb_{0.6}Ba_{.4}Nb_2O_6$ (PBN:) has a c lattice constant close to the c constant close to the both a and c constants of PLZT, a possibility is to first deposit a PBN:60 layer on an SBN:60 and then deposit the PLZT film on this layer and repeat this process until we get the desired optical modulation in these films. Figure 4 summarizes our experimental approach for this concept. As shown in the Figure 4, additional layers of PBN:60 and PLZT may be deposited to achieve the desired optical modulation. For spatial light modulators and guidedwave optics, it is advantageous for the films to have an optical refractive index larger than the substrate, while still maintaining a large optical figure-of-merit (r_{ij}/ε and n^3r_{ij}/ε). Both PLZT and PBN:60 possess a significantly higher index than SBN, with Δn of around 0.05 to 0.1.

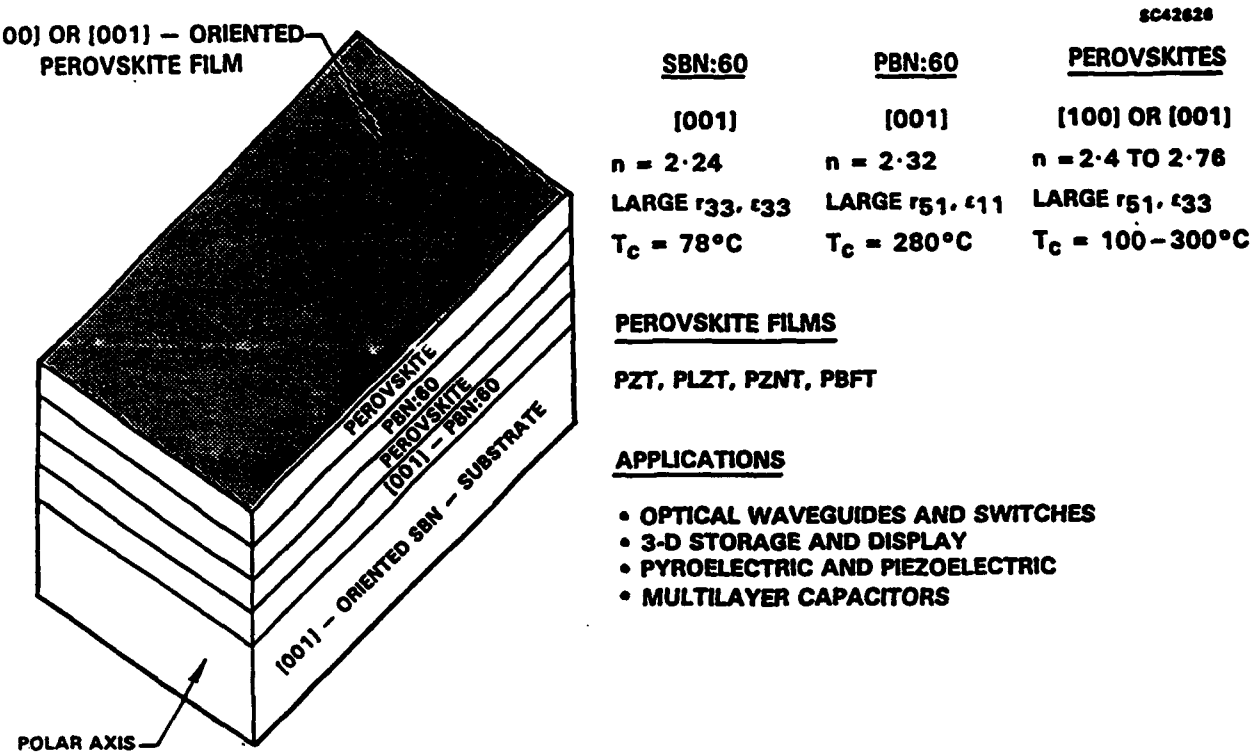

Figure 4: Multilayer Ferroelectric Thin Film Concept for Optical Applications

ACKNOWLEDGEMENT

This work was supported by the ARPA and by Rockwell International Independent Research and Development programs. The authors are grateful for discussions on this work with W. F. Hall and W. K. Cory.

REFERENCES

1. G. H. Haerting and C. E. Land, J. Am. Ceram. Soc. 54, 11 (1971).

2. K. Tanaka, Y. Higuma, K. Wakino and M. Murata, J. Am. Ceram. Soc. 59, 465 (1976).

3. Y. Matsui, Y. Higuma, M. Okuyama, T. Nakagawa and Y. Hamakawa, Proc. Ist Meeting of Ferroelectric Mat. and Their Applications (FMA Office, Kyoto, 1978) P.37.

4. Y. Hamakawa, Y. Matsui, Y. Higuma, and T. Nakagawa, Tech. Digest, IEEE IEDM, Washington, DC, 297 (1977).

5. W. E. Perry and B. M. Soltoff, Ferroelectrics, 10, 201 (1976).

6. C. E. Land and W. D. Smith, Appl. Phys. Lett. 23, 57 (1973).

7. S. G. Varnado, W. D. Smith, IEEE J. Quant. Electron. EQ-8, 88 (1972).

8. A. Kuwamada, K. Suzuki and G. Toda, Ferroelectrics, 10, 25 (1976).

9. K. Tanaka, Y. Higuma, K. Yokoyama, T. Nagakawa and Hamakawa, Jpn. J. Appl. Phys. 15, 1381 (1976).

10. M. Ishida, H. Matsunami and T. Tanaka, J. Appl. Phys. 48, 951(1977).

11. M. Ishida, S. Tsuji, K. Kimura, H. Matsunami and T. Tanaka, J. Cryst. Growth, 45, 393 (1978).

12. A. Okada, J. Appl. Phys. 49, 4495 (1978).

13. T. Nagakawa, J. Yamaguchi, T. Usuki, Y. Matsui, M. Okuyama, and Y. Hamakawa, Jpn. J. Appl. Phys. 18, 897 (1979).

14. Y. Higuma, K. Tanaka, T. Nakagawa, T. Kariva and Y. Hamakawa, Jpn. J. Appl. Phys. 16, 1707 (1977).

15. M. Okuyama, T. Usuki and Y. Hamakawa, Appl. Phys. 21, 339 (1980).

16. A. A. Ballman and H. Brown, J. Cryst. Growth , 1, 393 (1967).

17. R. R. Neurgaonkar and W. K. Cory, J. Opt. Soc. Am, B3(2), 274 (1986).

18. R. R. Neurgaonkar, W. K. Cory, J. R. Oliver, M. D. Ewbank, and W. F. Hall, Opt. Eng., 26(5), 392 (1987).

19. R. R. Neurgaonkar, I. Santha, J. R. Oliver, E. T. Wu and L. E. Cross, J. Mat. Science, 25, 2053 (1990).

APPENDIX 5.4

Applications of Ferroelectric Thin Films to Components of Optoelectronic Computing Systems

APLICATIONS OF FERROELECTRIC THIN FILMS TO COMPONENTS OF OPTOELECTRONIC COMPUTING SYSTEMS

S. H. LEE, V. H. OZGUZ, S. KRISHNAKUMAR, J. MA and Y. FAINMAN
University of California, San Diego, ECE Dept.
La Jolla, CA 92093-0407

ABSTRACT

System, device and material issues for the use of ferroelectric ceramic thin films in the realization of smart spatial light modulators and optical storage devices are considered. Results show that ferroelectric thin films such as PLZT, PBN, KTN, and SBN are particularly attractive.

INTRODUCTION

In recent years extensive efforts have gone into the development of components and modules for the realization of massively parallel optoelectronic computing systems.[1,2] These systems, where electronic and optical technologies are used in a balanced mixture, will overcome the limitations resulting from all optical or all electronic implementations.[2] In these development efforts, bulk materials such as ferroelectric materials, in which electrical and optical fields can interact, play a central role. For example, a ferroelectric oxide material, Lead Lanthanum Zirconate Titanate (PLZT), has been successfully used to realize smart spatial light modulators (S-SLMs) by combining bulk PLZT with silicon electronic circuits.[3,4] Another bulk ferroelectric material, Strontium Barium Niobate (SBN), has been studied for holographic storage.[5,6,7]

Thin films of these ferroelectric materials are particularly attractive for their potential use in integrated form with bulk silicon which is essential for electronic circuits. Thin films can be deposited on areas as large as several hundreds cm^2. When the deposition processes and subsequent modulator definition steps are made compatible with Si batch fabrication steps, the resulting S-SLM will become more manufacturable and the cost of fabrication will be reduced. In the following, we will outline the material requirements from systems viewpoint and will report unique approaches to exploit the properties of the ferroelectric materials by using them in components of optoelectronic computing systems.

COMPONENTS OF OPTOELECTRONIC COMPUTING SYSTEMS

The computational performance requirements of computers have continued to increase in recent years. In many computationally intensive applications such as large scale linear and non-linear algebraic modeling, data-base/knowledge-base systems, artificial intelligence and real time pattern recognition, the expected throughput requirement will exceed the range of 1-10 Tops/sec by the end of the decade. The throughput is proportional to the number and speed of the processing channels. Hence, higher throughputs requires high speed and/or parallelism. The speed of processing channels is limited by fundamental physical laws which govern operations of the constituent devices. Furthermore, increased number of cascaded devices in each processing channel results in delays and degraded performance. A highly parallel computer uses the parallelism along with speed and consists of a large number of processing elements (PE) operating in parallel. The speed constraints can be relaxed as the number of PEs increases. However, the use of many parallel PEs increases also the communication needs among PEs. If one attempts to build highly parallel computers with conventional electronic implementations, highly parallel communication can not be supported due to interconnection bottleneck. The bottleneck is a direct consequence of the technological limitations of electrical interconnections in terms of area, latency and power dissipation. The area problem results from the planar nature of the electronic technologies. Unless enough spatial separation is provided, independent information carrying electrical channels interact, which results in excessive crosstalk. The latency and power problems are also an inherent result of the properties of electrons which are relatively slow and which require relatively large amount of control energy for long distance routing.

One way to solve these problems is to use the inherent parallel nature of optical energy fields. Optical beams can crossover each other without crosstalk, owing to the properties of the photons. Hence, a flexibility in the interconnection is introduced by using fully the 3-D space available for processing.[8] Since a highly parallel computer architecture usually requires a mixture of local and global interconnection, a more powerful approach to implement a parallel computer is to use an optimal mixture of electronics and optical technologies for satisfying high parallelism needs and in the same time, minimizing the energy consumption in the system. Such an optoelectronic computing architecture would consist of many PEs, interconnected globally by using free space optical interconnections. The use of optical interconnections eliminates the communication bottleneck due to their inherent high bandwidth and parallel nature. Furthermore, free space optical interconnections with their three dimensional features overcomes the problems resulting from planar technology.

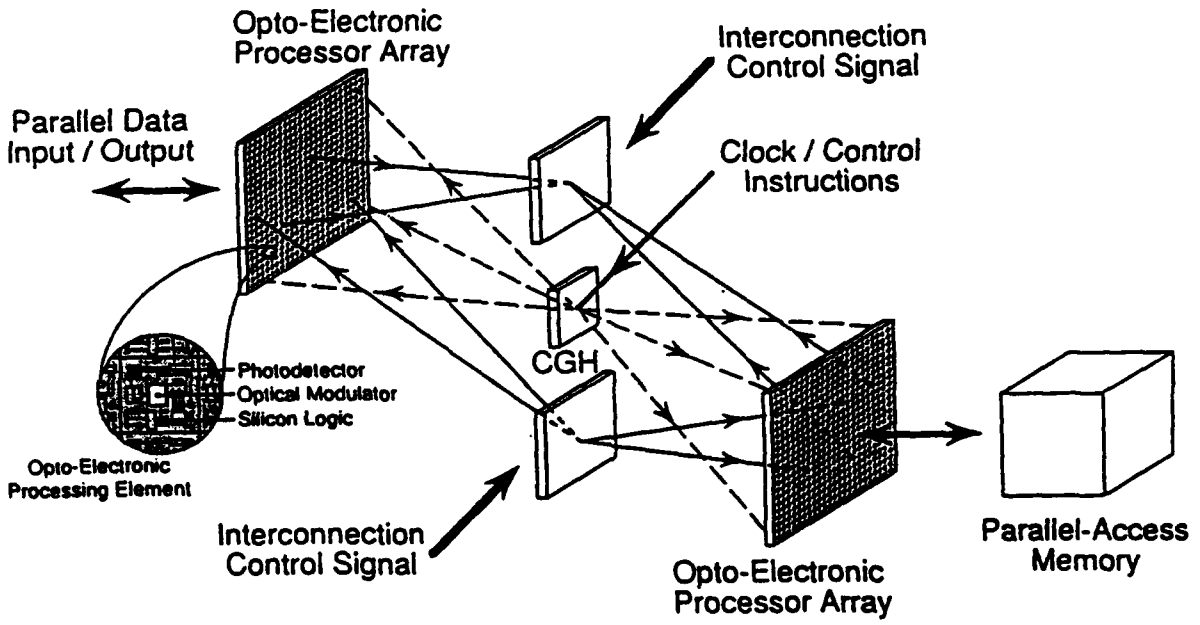

Figure 1. The architecture of the Programmable Opto-Electronic Multiprocessors (POEM) system.[2]

An optoelectronic computing architecture proposed by UCSD is illustrated in Figure 1.[2] As can be seen in the figure, the major constituents of the opto-electronic computing system are: PEs with optical I/Os, fixed or reconfigurable free space optical interconnection elements between the PE planes and highly parallel optically accessed memories. Free space optical interconnections permit the reconfigurability of the interconnection network, which is not easily done with electronics. Reconfigurability is achieved by varying the the beam routing functions of the optical elements used for interconnections, and can be performed by photorefractive materials. Information processing tasks are carried out by conventional electronic circuits in the PEs. To provide parallel optical I/Os, devices controlling various properties of the optical fields are needed. Spatial Light Modulators (SLMs) are devices capable of modifying the amplitude (or intensity), phase or polarization of an optical wavefront as functions of the spatial position and time.[3] The memory function can be performed using the

photorefractive properties of materials. Photorefractive devices with large information storage capacity and write-erase capabilities are also needed. Optically interconnected electronic parallel computing systems offer the potential of 2-3 order higher performance compared to all electronic approaches.[10]

Ferroelectric thin films, owing to their linear, quadratic and/or higher order electro-optic effects, have the potential of fulfilling many expectations for the realization of the memory, reconfiguration and modulation devices. Furthermore, the use of thin films of ferroelectric materials allows the integration with other materials and therefore is crucial for compact system packaging. However, the expectations from these films such as thickness requirements, electro-optic coefficients can not be easily met and new approaches are needed. These expectations will be detailed in the following sections.

FERROELECTRIC THIN FILMS IN SMART SPATIAL LIGHT MODULATORS

A Spatial Light Modulator (SLM) was previously defined as a device capable of modulating the characteristics of an optical field. SLM consists of two major functional sections: i) the control section which is electrical or optical, ii) the readout section which must be made of a material capable of changing some properties of an incoming beam (i.e. amplitude, phase or polarization) with the information provided from the control section.

Local information processing power can be added to each pixel of a spatial light modulator between the control and read-out sections to enable their usage in an architecture such as one described in Figure 1. Such spatial light modulator array, where a 2-D optical field is modulated depending on the decision obtained in the local processing unit from the input data, is a unique approach for computing; it can be called Smart Spatial Light Modulators (S-SLM).[3,4] Incoming control signals can be optical and are sensed by light detectors. These detectors convert the control signal into electronic form that is then fed to an electronic circuit for local processing. The control signals for the electronic circuit can also be transmitted electrically. In principle, the electronic circuit of each pixel in an S-SLM can be as simple as a logic gate with a few transistors or as complex as a programmable processor (PE) with a few thousand logic gates. At the output of the PE, the processed data is converted back into optical form via light modulators, and is then routed to another PE with free space interconnection optics.

S-SLMs can be categorized with respect to the geometry of the incoming and outgoing optical beams as well as the type of the modulator used. Hence we can distinguish single or double sided, reflective or transmissive S-SLMs.

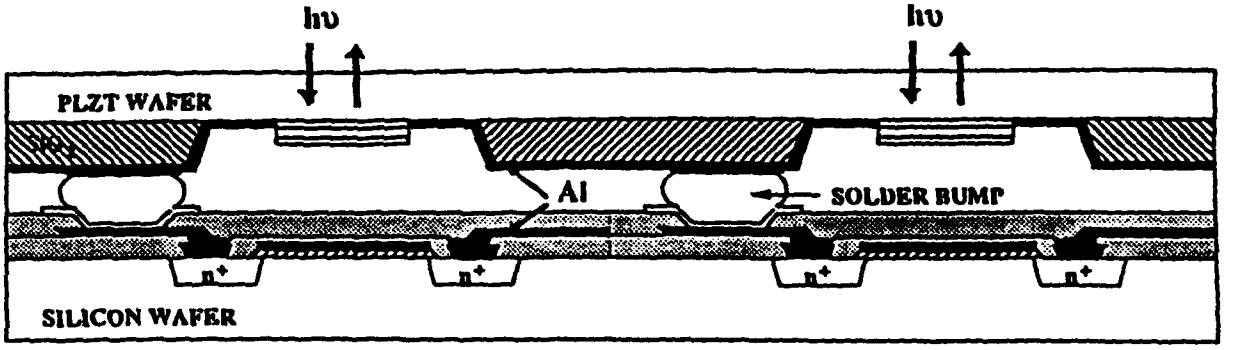

Figure 2. Hybrid double-sided reflective Si/PLZT Smart SLM based on flip-chip bonding.

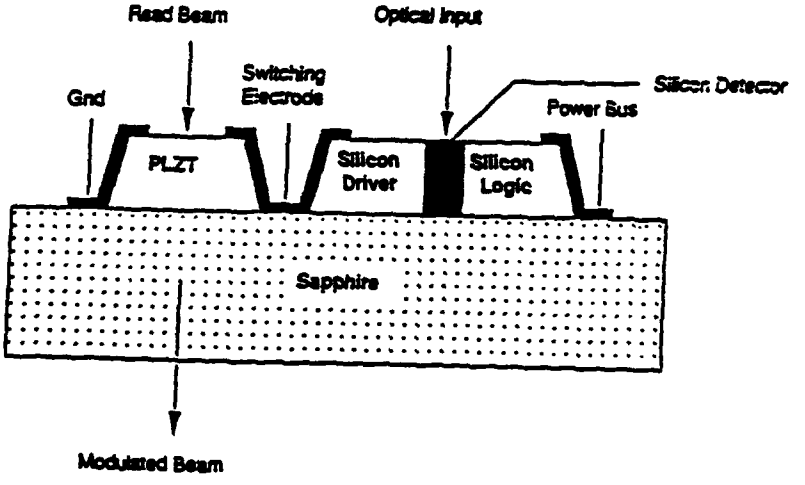

Figure 3. The cross section of a double-sided transmissive thin film Si/PLZT smart SLM.

From a system viewpoint, double sided geometries, where incoming and outgoing beams are at each side of a common substrate, provides design flexibility. However, single sided reflective S-SLM offers the advantage of allowing thermal cooling/assembly on the unused side.

For S-SLMs, electronic processing circuits and detectors in silicon can to be combined with light modulators on a ferroelectric material. Bulk forms of ferroelectric materials can be flip-chip bonded to to silicon resulting in the hybrid structure shown in Figure 2. For further integration, thin film forms of ferroelectric materials are needed, as shown in Figure 3. Thin film deposition of ferroelectrics allows the integration with any complexity of VLSI circuits.

System Requirements for S-SLM

In order to build efficient S-SLMs, modulators with high contrast ratio (ON state signal/OFF state signal) and high optical throughputs are required. Improvement in the contrast ratio can be achieved by not only improving the ON state signal, but also through lowering of the OFF state signal. However, for electro-optic modulators, the ON state signal should not be increased by simply increasing the applied voltage because high voltages require complicated and slow drive circuitry limiting the scalability. The OFF state signal can not be lowered beyond the noise limits (e.g. background optical noise level, device noise levels). Besides the contrast ratio, the absolute power at ON state needs to be selected to insure adequate a signal to noise ratio (SNR) or bit error rate (BER). Furthermore, inadequate absolute optical power levels requires sophisticated sense circuits with large transistor counts, thus sacrificing the scalability. Speeds in the order of at least 1 MHz is needed to efficiently exploit the benefits of parallelism.[10] Lowering of device capacitance and operating voltage in the system would reduce the switching energy, thereby allowing larger PE array and higher operation speeds. Lower operating voltages become also an important prerequisite for monolithic integration.

Modulator materials with low optical absorption would reduce the optical power requirements of the system and relax heat dissipation constraints. Consequently, modulators which work on optical absorption principle (e.g. MQW based SLMs [3]) have typical problems related to heat dissipation during the OFF state, where the material is inherently absorbing all the incoming optical power. The need for low absorption is especially important for the optical fan-out capabilities of the modulator. In many practical applications, fan-out in the range of 2-20 is required. Some applications such as neural networks have even higher fan-out requirements. Since the optical power is split into several beams by the fan-out of modulators, more total optical power is required to satisfy the sensing conditions at the detector level. Increase in the optical power will be limited, however, by the heat dissipation during the OFF state for absorption type modulators such as MQWs. Light sources, which are potential candidates as an alternative to modulators, are suffering from the same heat dissipation disadvantages for large fan-out requirements. In summary, typical expectations from a S-SLM would be:

contrast ratio > 10:1	capacitance: < 1pF/modulator
switching speed: > 1MHz	operating voltage < 20-30 V (5V preferred)
switching energy: < 2000 fJ/cm^2	fan out > 2 (>10 preferred)

In order to maximize the number of PEs and still stay within the limits imposed by the constraints shown above, care has to be taken with regard to the choice of the modulator material in terms of their electro-optic coefficient, switching energy, spectral width, latency, and dynamic range. Most of the ferroelectric materials are inherently fast and the switching speed of the modulator is limited by electronic drive capabilities for high voltages. Other modulator materials requiring low voltages are slow. Unless the number of modulators can be significantly increased to maintain system processing throughput, such materials should also be avoided. Fast electro-optic materials requiring lowest drive voltages and switching energies seem to be best suited for S-SLMs for parallel computing modules.

Material Requirements for Smart Spatial Light Modulators

These system/device requirements can be translated to material requirements. The optical phase retardation γ (in radians) is given by

$$\gamma = \frac{2\pi t}{\lambda_0}(\Delta n) \tag{1}$$

where Δn is the difference between the principal refractive indices normal to the direction of propagation, λ_0 is the wavelength of light in vacuum, and t is the optical path length (thickness of the film). Therefore, we must choose the thickest film with the largest difference between indices of refraction to obtain maximum retardation (i.e. $\gamma = \pi$). These conditions have direct implications on the deposition of the thin films.

Ferroelectric oxide materials with strong electro-optic effect (i.e. large difference between refractive indices under applied electric field) are PLZT, KTN, SBN, and PBN. The effect of saturation of electro-optic effect with applied electric fields needs to be taken into account when using these materials in actual devices. In this respect, SBN seems to show saturation of E-O effect at higher fields as compared to PLZT and could hence be more useful. Below the curie temperature, SBN, KTN, and PBN have three independent nonzero moduli $r_{13} = r_{23}$, $r_{42} = r_{51}$, r_{33}. Due to assymmetry, the orientation of crystal axis with respect to the electrical field and light propagation becomes important.

Case 1: For electric field parallel to c-axis and light parallel to the a-axis, it can be shown that for point group 4mm

$$n_2 = n_0 - n_0^3 r_{13} \frac{E}{2} \tag{2}$$

$$n_3 = n_e - n_e^3 r_{33} \frac{E}{2} \tag{3}$$

where n_2 and n_3 are the indices of refraction perpendicular to a-axis (to light propagation), E is the field strength and n_0 and n_e are the ordinary and extraordinary indices of refraction respectively.

Case 2: For the electric field parallel to the a-axis and light parallel to the c-axis, it can be shown that,

$$n_1 = n_0 - n_0^3 r_{51}^2 \frac{E^2}{2\left[\frac{1}{n_0^2} - \frac{1}{n_e^2}\right]} \tag{4}$$

$$n_2 = n_e \tag{5}$$

where n_1 and n_2 are the refractive indices perpendicular to the c-axis (to light propagation).

For SBN, *Case 1* yields a fairly large E-O effect since r_{33} is large, whereas *Case 2* yields a low E-O effect since r_{51} is low. Therefore, for modulator application where the light propagation is perpendicular to the substrate, it would be best to deposit SBN with c-axis parallel to the substrate (a-axis perpendicular to the substrate) and apply a transversal field (i.e. *Case 1*). However, the lattice constants of SBN are different along a- and c-axes, due to the non-symmetry of the structure (i.e. a = 12.43 Å and c = 3.91 Å). Hence, it would be difficult to deposit defect-free, good quality and uniform thin films where long lattice sites (a-axis) are perpendicular to the substrates such as silicon, GaAs or sapphire. Although *Case 2* seems to yield smaller electro-optic effect the increase in the denominator of Equation (7) (difference of n_0 and n_e) can increase the optical phase retardation. The difference is expected to decrease due to the stresses induced during the deposition of thin films owing to differences of the lattices of the substrate and the film.

For PBN and KTN r_{33} is low and r_{51} is high; *Case 2* yields a higher electro-optic effect. For PLZT the electro-optic effect lies intermediate to that of SBN and KTN in both cases,

since the a- and c- axis orientation during deposition do not affect the electro-optic properties due to its quasi-cubic crystal structure.

During our initial explorations we have found that PLZT seems to satisfy the majority of SLM requirements. PLZT (9/65/35) exhibits a large quadratic electro-optic effect, requiring relatively small modulation voltage at the expense of a large dielectric constant which increases required switching energy but still within manageable limits. It is also commercially available in wafer form up to 6 inches in diameter. In addition, PLZT can be deposited in a thin film form on various substrates including silicon and sapphire. Hence, PLZT offers promise for monolithic integration. Since silicon appears to be the optimum material for the detection and logic operation part of the S-SLM, in the following we will concentrate on Si/PLZT based S-SLM technologies involving thin PLZT films.

Integration Technologies For Si/PLZT S-SLM

A straightforward approach for combining silicon with PLZT is hybrid integration technique such as flip-chip bonding used in silicon packaging technology (Fig. 2). This technique is well developed and can be used to increase the S-SLM yield by preselecting working PEs. However, it is costly for large arrays. The scalability of S-SLMs can be improved with monolithic integration techniques. The monolithic integration of two different materials usually involves thin films of one material deposited or bonded onto the other material. Hence, three approaches were followed to integrate silicon on PLZT [11]. The first approach involves the deposition and subsequent seedless recrystallization of a polysilicon film on a PLZT substrate. Electronic circuits are then fabricated in recrystallized silicon. A second approach uses thin, bulk quality silicon films bonded to PLZT substrates. In the third approach, a thin film PLZT film is deposited in windows on a silicon-on-sapphire (SOS) substrate. Sapphire is an excellent choice of substrate to build high density silicon-on-sapphire electronic circuits, thus allowing monolithic integration. All of these techniques have been investigated at UCSD, and have played important roles in the advances of S-SLM technologies. In comparison, the processing power of the S-SLMs fabricated using laser recrystallization of silicon is limited, ultimately, by the quality of the silicon film after recrystallization. That is, the number of transistors in a PE will be restricted, imposing constraints on the size and complexity of the PE. The quality of silicon in the bonding approach is very high thus allowing higher yields and increasing the scalability of the approach. Development work to establish a more reliable bonding technique is underway. Deposition of ferroelectric thin film PLZT on windows opened on the SOS wafer can provide more processing power by implementing silicon devices on the substrate prior to the deposition of PLZT films. CMOS VLSI circuits of any complexity can be achieved and linked to PLZT light modulators on the same substrate. The use of transparent sapphire

substrate allows transmissive or double-sided reflective S-SLMs. Without a transparent substrate, this flexibility can not be obtained. Figure 3 shows the cross-section of the silicon/PLZT on sapphire SLM. The critical step towards the development of such a device is, therefore, the growth of PLZT films of the right composition and crystallinity on the appropriate sapphire substrate. The r-plane ($1\bar{1}02$) sapphire was chosen as the substrate to provide compatibility with SOS technology. The shortcoming of this technique is the limit in the amount of light modulation that can be achieved due to the limited thickness of the PLZT films obtainable on sapphire. However, light modulation can be improved dramatically by placing the film in a Fabry-Perot interferometer. Such an interferometer would also offer attractive features such as high speeds (due to low intrinsic capacitance) and low switching energies. A different approach would be to exploit the properties of multilayers of ferroelectric films. The following sections will deal with various aspects involved in the deposition of PLZT films including the characterization of their composition, crystallinity, electrical and electro-optical properties, and evaluation of the suitability of various approaches for developing silicon/PLZT S-SLMs.

Properties of Thin PLZT Films Deposited on Sapphire

The system used for depositing PLZT on sapphire is a triode sputtering system. It uses two R-F triode magnetron sputter sources and one Ion gun with low energy Ar ions to permit pre-deposition substrate cleaning in a planetary configuration. The r-plane sapphire substrate was epitaxially polished on the front face (the face of film growth) and optically polished on the back face and mounted on a rotating molybdenum block using molten indium. The molybdenum block was heated on the back side with halogen lamps. The substrate temperature was monitored using a Chromel-Alumel thermocouple attached to the substrate holder close to the sample. The system parameters and sputtering conditions used in the experiment are summarized elsewhere.[12] Experiments were performed using various target compositions, sputtering power and substrate temperature.

To measure the electrical and electro-optical properties of the films, aluminum was deposited by thermal evaporation on the films, and patterned using photolithography to form an interdigitated electrode structure (IDE) of varying finger widths (ranging from 15 to 40 μm) and electrode center to center spacing of 55 μm. Optical transmission characteristics of the films were evaluated using a spectrophotometer. The thickness of the films were obtained using Rutherford backscattering spectroscopy and correlated using ellipsometry at various wavelengths. Electro-optic coefficient of the films, was measured by using a coherent light at 514 nm polarized 45° with respect to the electric field applied to the film. Compositional Analysis of the film were performed by Rutherford Backscattering Spectrometry (RBS) using a

2.3 Mev He^{++} beam. Analysis on bulk PLZT samples of known composition were performed to establish a baseline for comparison. Thin film samples, both as-deposited and after post deposition anneal, were analysed and the experimentally obtained spectra was superimposed over the spectra simulated for the case of PLZT (9/65/35) on sapphire. Auger Electron Spectroscopy (AES) was also used to correlate the results of RBS to obtain accurate information about the compositional uniformity of the film as a function of depth from the surface. Good correlation was observed between RBS and AES analysis. By holding the substrate temperature to 500°C and adjusting the composition of the PLZT target before the deposition, we were able to accurately control the composition of the PLZT film (see Figure 4).

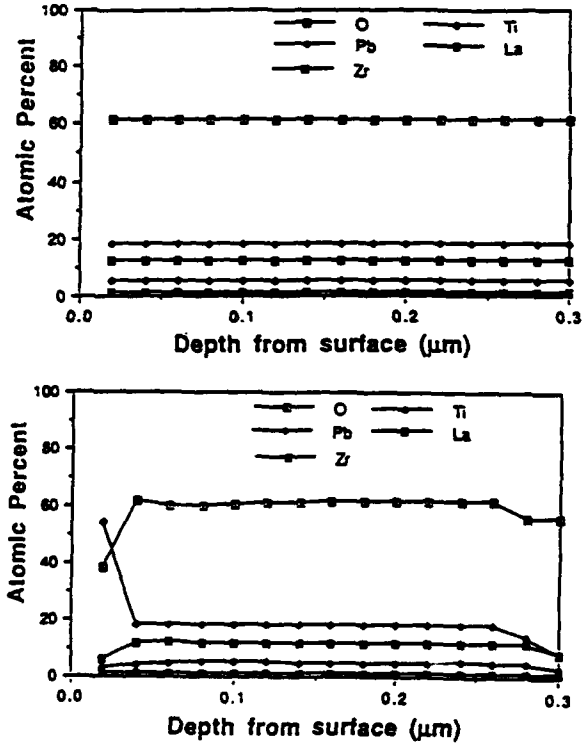

Figure 4. Auger analysis results for, a) bulk 9/65/35 PLZT, b) sputtered 9/65/35 PLZT thin film.

The composition of the deposited film closely matched that of the bulk ceramic. Crystallographic studies, performed using X-ray diffraction employing CuK_α radiation, revealed that the films had a crystalline structure with a dominant (110) orientation.

The dielectric constant of the film ε_f was estimated from the measurements on the capacitance of the IDE using the following equation:[13]

$$C = K N l\{(\varepsilon_s+1) + (\varepsilon_f - \varepsilon_s)\,[1 - \exp(-4.6t/L)]\} \quad (6)$$

where K is the constant given by the structure of the IDE, N is the number of fingers in the IDE, l is the finger length of the IDE, ε_s is the dielectric constant of the substrate, t is the film thickness and L is the center-to-center spacing between adjacent fingers of the IDE. Using this method the dielectric constant of the perovskite films, after annealing, were estimated in the range of 1500-2500 (at 10 KHz), whereas the as-deposited pyrochlore films had a dielectric constant in the range 10-100. The improvement of the dielectric constant, after annealing and for compensated films, is another indication of the success of these techniques. The dielectric constant tends to decrease at higher frequencies. A similar effect was observed in our measurements on bulk samples. A plot of the dielectric constant as a function of temperature at 10 KHz to 1 MHz frequency range is shown in Figure 5. The dielectric constant shows an anomaly at around 220°C. The Curie temperature thus obtained is larger than that reported for bulk samples.[14] This could be due to microscopic changes in the crystal structure of the films as compared to the bulk ceramics.

A plot of the light transmission versus wavelength is depicted in Figure 6. The transmission curve has been normalized with respect to the sapphire substrate.

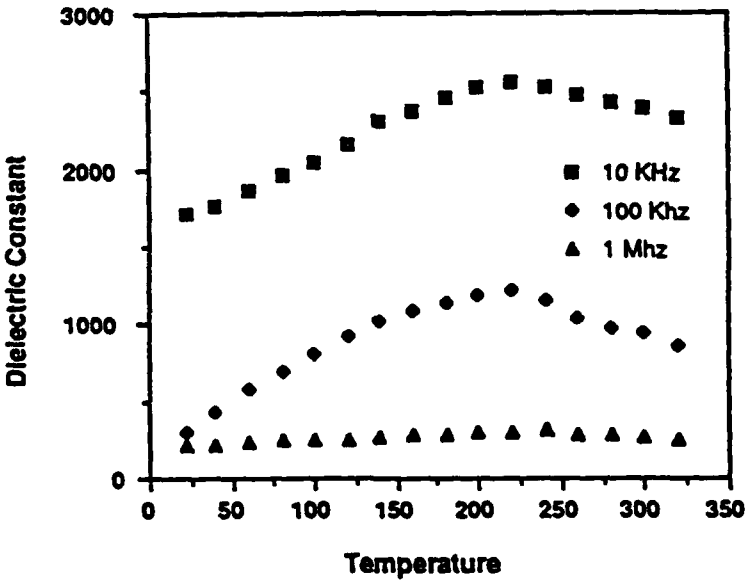

Figure 5. Dielectric constant of thin film 9/65/35 PLZT as a function of the measurement temperature at various frequencies.

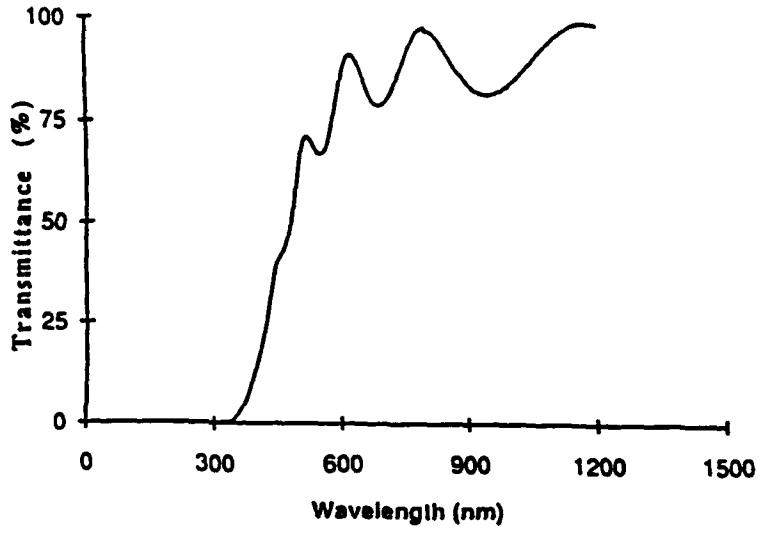

Figure 6. Optical transmission of thin 9/65/35 PLZT film as a function of the wavelength.

The transmission increases after 0.35 μm and shows interference oscillations corresponding to the flat surface of the film and PLZT/Sapphire interface. The peaks of these interference oscillations correspond closely to the substrate transmission indicating low absorption and scattering losses. Simulations were performed to evaluate the dispersion curves and absorption characteristics of the PLZT films. These simulations modeled the light transmission through the structure consisting of a PLZT film of appropriate thickness deposited on a sapphire substrate. Figures 7 and 8 show the plots of refractive index and absorption versus wavelength.

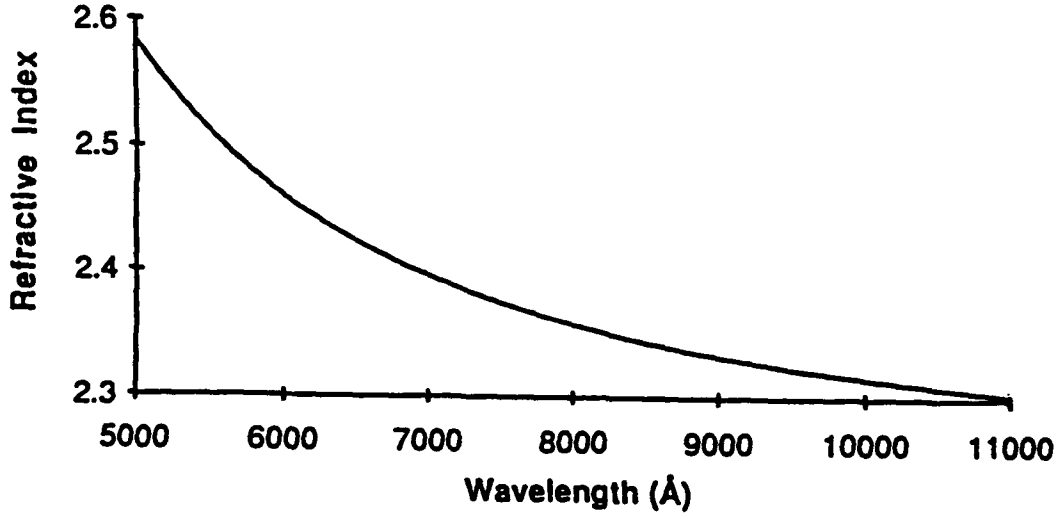

Figure 7. Refractive index of thin film 9/65/35 PLZT film as a function of the wavelength.

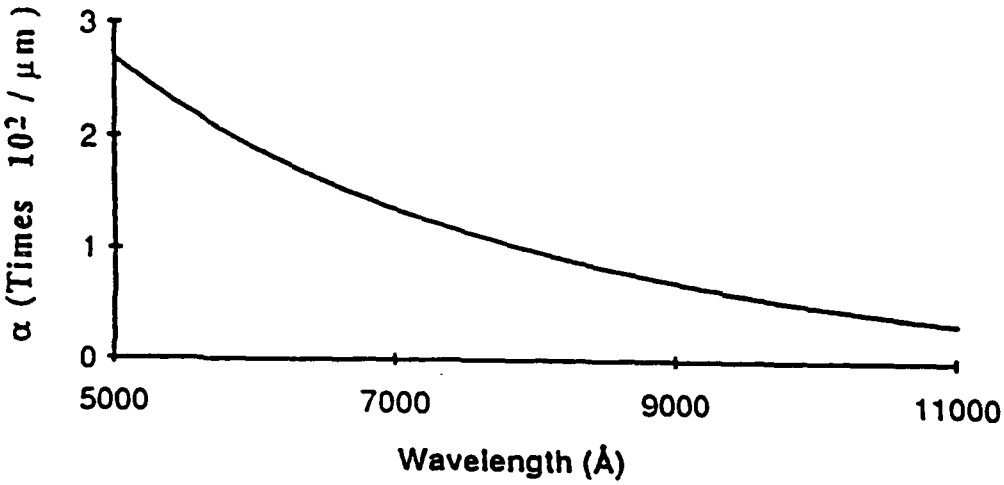

Figure 8. Optical absorption of thin film 9/65/35 PLZT as a function of the wavelength.

Generally a Sellmeier dispersion relationship fits the dispersion of the refractive index for a large number of dielectric materials:[15]

$$n^2 - 1 = \frac{S_0 \lambda_0^2}{(1 - \frac{\lambda_0^2}{\lambda^2})} \tag{7}$$

where n is the refractive index , S_0 represents the oscillator strength and λ_0 the position of an average oscillator. The PLZT films show extremely good correlation with Sellmeier dispersion formula for the case of a single electronic oscillator. Similar agreement has been found for the case of bulk PLZT (9/65/35) as well as for PLZT films deposited by other workers.[16,17] In fact the values of S_0 and λ_0 estimated at 56.514 μm^{-2} and 267.7 nm respectively were found to be in close agreement with the values for bulk PLZT (9/65/35).[16]

To measure the electro-optic effect in the films, an electric field was applied on the IDE. Application of the electric field causes a birefringence Δn in the film. This causes a rotation in the polarization of the incoming light. The resultant polarization rotation is detected using two detectors monitoring the intensity of the orthogonal polarization states. By obtaining the difference in the intensity of the orthogonal polarization states before and after application of the electric field, one can obtain Δn from the following equation.[18]

$$I = 2 \sin^2(\frac{4\pi t}{\lambda} \Delta n) \tag{8}$$

where I is differential intensity in the two polarization states caused by application of the electric field, t is the thickness of the film, and λ the wavelength of light used. Δn can be related to the electro-optic coefficient R by

$$\Delta n = -\frac{1}{2} n^3 R E^2 \tag{9}$$

where R is the quadratic electro-optic coefficient of the film, n is the refractive index of the film, and E is the electric field applied on the film. A plot of the change of birefringence as a function of applied electric field is shown in Figure 9. The electro-optic coefficient R was calculated to be 0.6×10^{-16} m^2/V^2.

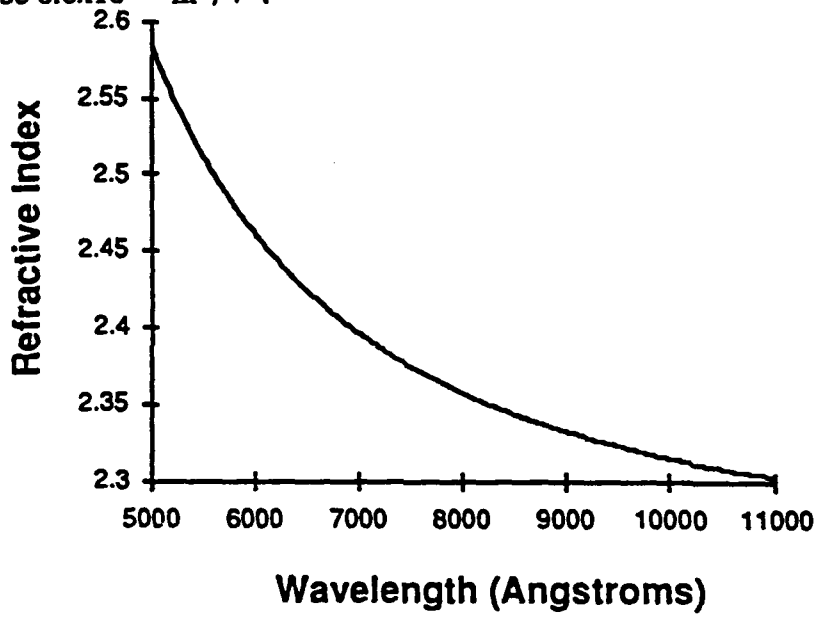

Figure 9. Birefringence of thin film 9/65/35 PLZT film as a function of the applied electric field.

When used in SLMs, the dynamic range of the modulator is related to the effective change in refractive index as well as the thickness of the film. Assuming the value of electro-optic coefficient of the films is 0.6×10^{-16} m^2/V^2 and an electric field of 2 V/μm, we would need a PLZT film 25 μm thick in order to obtain a modulation depth of 40%. Film thicknesses larger than few μm are difficult to obtain by using physical deposition techniques such as sputtering. New and emerging techniques such as metallo-organic chemical vapor deposition (MOCVD) are promising for realizing thicker ferroelectric films provided that the precursors for reaction are developed.

Ferroelectric Thin Films in Fabry-Perot Cavities

Thin film ferroelectric ceramics have been successfully obtained with electro-optic coefficients approaching bulk values.[12,13] However, due to their limited thicknesses, the total modulation effect, which is linearly dependent on the optical path in the ferroelectric material, is lower than that of bulk materials for a given applied voltage. The first solution to this problem is to place thin film in an interferometric cavity (Fabry-Perot) to increase the effective total optical interaction path. Fabry-Perot thin film modulators offer the advantage of higher operation speeds due to their lower capacitance. Such a Fabry-Perot modulator would consist of the PLZT film bounded by two reflective layers on sapphire. The finesse of the modulator, adjusted through changes in the mirror reflectances, would control the wavelength spread over which the modulator would be effective. The finesse also decides the control needed on the thickness of PLZT film over the substrate. A plot of the simulation of the reflected intensity as a function of voltage applied on the Fabry-Perot modulator is shown in Figure 10.

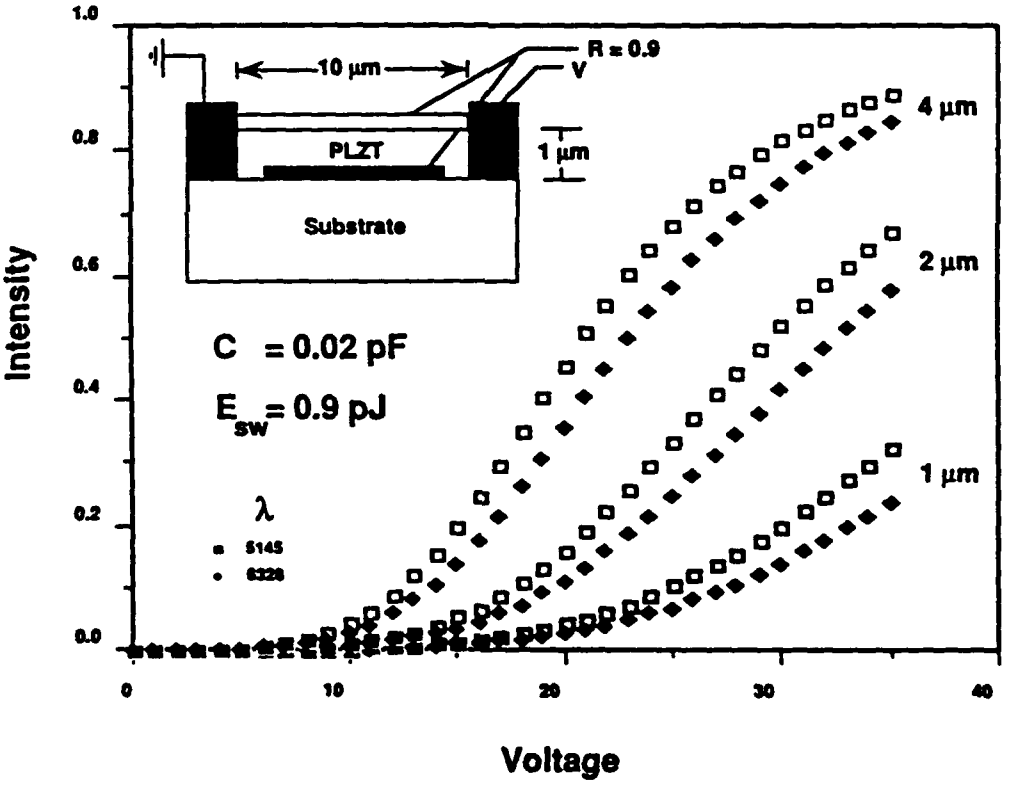

Figure 10. The simulation of optical modulation using thin PLZT film in a Fabry-Perot modulator.

The results points to 14% modulation at 20 V swing and is satisfactory for system requirements. However, Fabry-Perot modulators suffers from the following drawbacks: i) the fabrication and operation characteristics needs to be very tightly controlled (less than 0.5% variation in the thickness of the thin film is required), ii) the mirror material between the substrate and

the thin film needs to have high reflectivity (about 90%) and be compatible with the ferroelectric material growth. The results of a simulation performed for a 2μm PLZT ferroelectric thin film placed in a Fabry-Perot cavity with varying mirror reflectivities are shown in Figure 11.

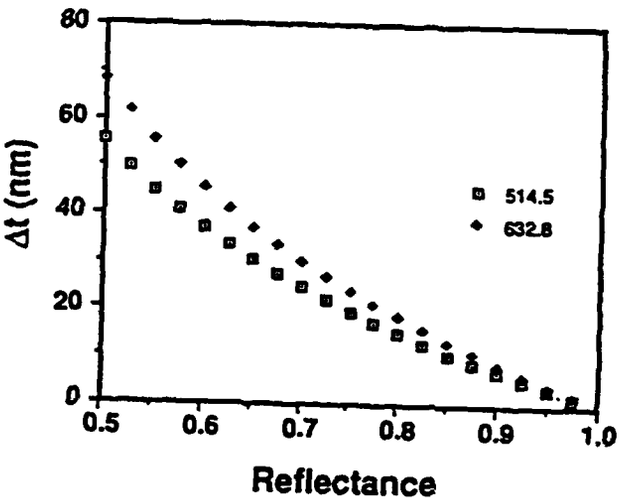

Figure 11. Thickness tolerance vs. mirror reflectivity for 2μm thick PLZT

The total thickness control required to maintain modulation performance within 3dB of the design value is less than 0.5%. On a 2μm film, this translates to a thickness that must be controlled within ± 10nm which, although hard, is not impossible to achieve. Indeed, the operation of Fabry-Perot ferrolectric thin film modulator is similar to that of a Fabry-Perot multiple quantum well modulator (MQW). The wavelength of the operation in Fabry-Perot cavities needs to be controlled to within a few nm. Hence, they suffer from similar drawbacks just mentioned. Moreover, MQW modulators are based on the excitonic absorption and the excitonic peak needs to overlap with the peak of the Fabry-Perot cavity for proper operation.[19] Consequently, thickness and operation wavelength control in MQW modulators becomes more crucial and temperature sensitivity increases. Furthermore, absorption based operation result in power dissipation in the off state, and the modulated light power becomes limited. To this extent, ferroelectric thin film Fabry-Perot modulators are more manufacturable and reliable than MQW modulators.

Recently, PLZT thin films have been deposited on platinum on sapphire. Figure 12 shows the reflectance spectrum of such structure which constitutes the base for future Fabry-Perot experiments.

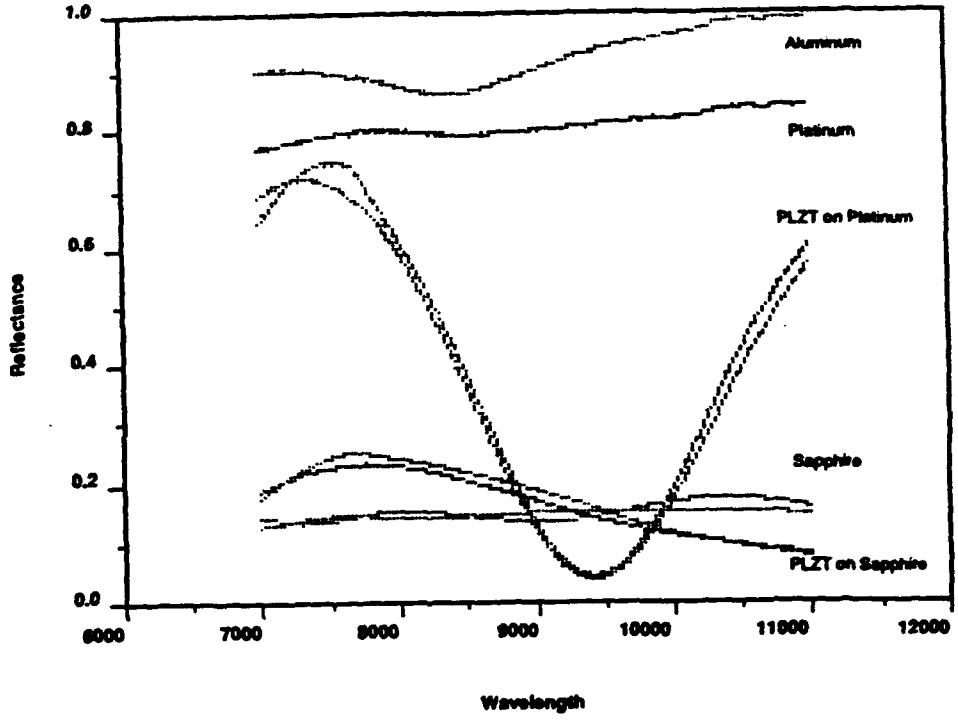

Figure 12. Reflectance spectrum of several materials including PLZT films on sapphire and on platinum.

The reflectance of the underlying platinum was of the order of 70%. The reflectivity at the air-PLZT interface based on the refractive index of PLZT is expected to be around 40%. Hence, the air-PLZT-platinum structure constitutes an etalon with very low finesse. Fabry-Perot effect is evident in the 750-950 nm range. Slight birefringence is also observed as shown in Figure 12 evidenced by the differences of reflectivity of two orthogonal polarization modes. For comparison, reflectances of aluminum, platinum, and sapphire are also included. If one were to choose materials such as gold or dielectric stacks possessing higher reflectivities (>90% at 5145 nm or 6328 nm) in place of aluminum and use a top mirror, it is possible to create a high finesse Fabry-Perot etalon using PLZT. This etalon will then exhibit higher optical contrast ratios for more useful operations in an S-SLM. The realization of this etalon necessitates the study of PLZT growth on alternate materials.

Multilayers of Ferroelectric Thin Films

Another way to increase the modulation is to use multilayers of ferroelectric thin films. If $\lambda/4$ thick alternating layers of two different type of ferroelectric materials is used, the resulting multilayer structure has a total reflectance vs. wavelength dependence which can be altered with the voltage applied to the stack as illustrated in Figure 13.

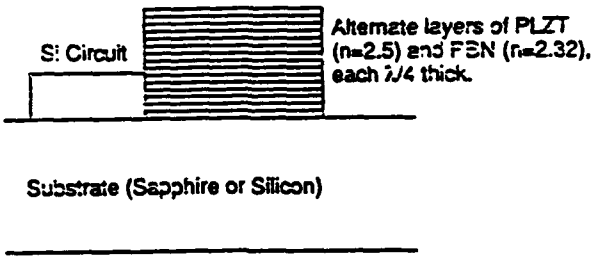

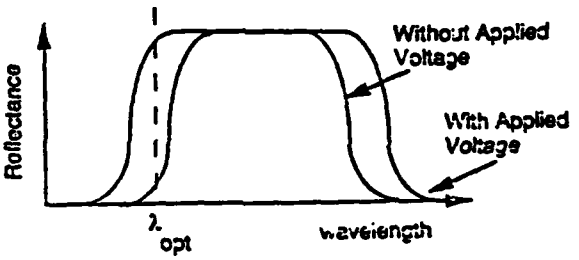

No Voltage ⇒ Stack reflectance high

Voltage (10V/μm) ⇒ Stack reflectance low

Figure 13. The concept of multilayered electro-optic thin film structures and change of the total reflectance of the stack with respect to the wavelength at two different voltages.

By applying field to the structure, refractive indices (ni) of constituent layers can be changed, effectively changing the optical thicknesses of each layer. The index modulation will shift the frequency response of the multilayer stack . Thus, for certain wavelength, the multilayer stack will cause virtually zero reflection at V = 0 and high reflection at some V >0. Such structure retains all the advantages of Fabry-Perot type modulators such as higher modulation depth (or contrast ratio), higher switching speeds and lower switching energies than modulators based on bulk materials because the total thickness of the thin film stack is few μm. Compared to MQW based modulators, the device formed by multilayer stack transmits the light through the substrate in the off-state relieving power dissipation requirements and

increasing the amount of light power that can be modulated. Furthermore, the thickness control and wavelength dependence requirements can be relaxed. Since the reflectance of individual layer controls the final performance of the stack, a simple in-situ reflectivity control can be added to the growth equipment to enable a precise control of thickness. In order to achieve effective multilayer ferroelectric modulators, the material selection in terms of constituents of the multilayer stack, the number of layer pairs, operating wavelength, index of refraction of the constituents, the selection of substrate, the selection of interface layers to enhance the reflection/transmission between the substrate and the multilayer stacks are all parameter affecting the optimization. We performed initial simulations based on two ferroelectric ceramic materials namely PLZT (n = 2.55) and PBN (n = 2.33) at 514 nm range because their thin film parameters were available for this wavelength. The value used for thin films are based on the results obtained from individual deposition of PLZT and PBN thin films.

A. Multilayer Design for Enhanced Tolerance

We have analyzed up to 10 layer pairs of PLZT and PBN and we considered two substrates, silicon and sapphire that are directly compatible with silicon based processing. The most promising result is obtained for silicon substrate with PLZT as initial layer and for 8 pairs (the total thickness is 0.8 μm) as shown in Figure 14.

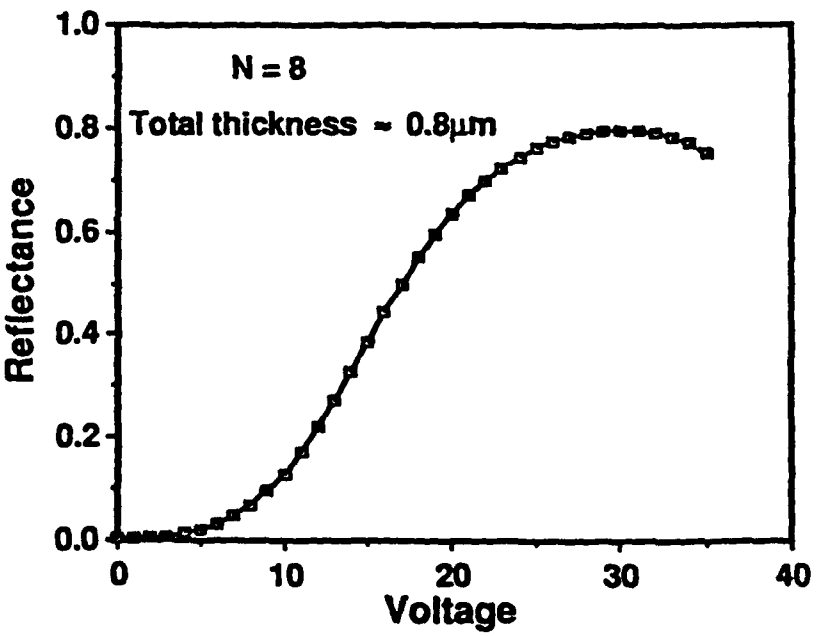

Figure 14. Simulation results for the reflectance of 8 pairs PBN/PLZT multilayer stack on silicon.

A reflectance variation of 70% (or contrast ratio of 90:1) can be obtained at 20 V. For comparison, 1 μm PLZT film can produce only 0.02% of reflectance variation and 1 μm PLZT film in Fabry-Perot with 0.9 mirror reflectivity yields 4% at 20 V. Asymmetric MQW modulator can achieve similar contrast ratio and modulation depth values at about 10 V applied voltage. However, the thickness control requirements are more severe. It has been reported that the thickness of the active layer in MQW based modulators needs to be controlled within 0.15% to achieve a 2.2 nm operating region centered at 865 nm.[19] Thickness sensitivity analysis in the 8 pairs multilayer stack on silicon is simulated and presented in Figures 15 and 16.

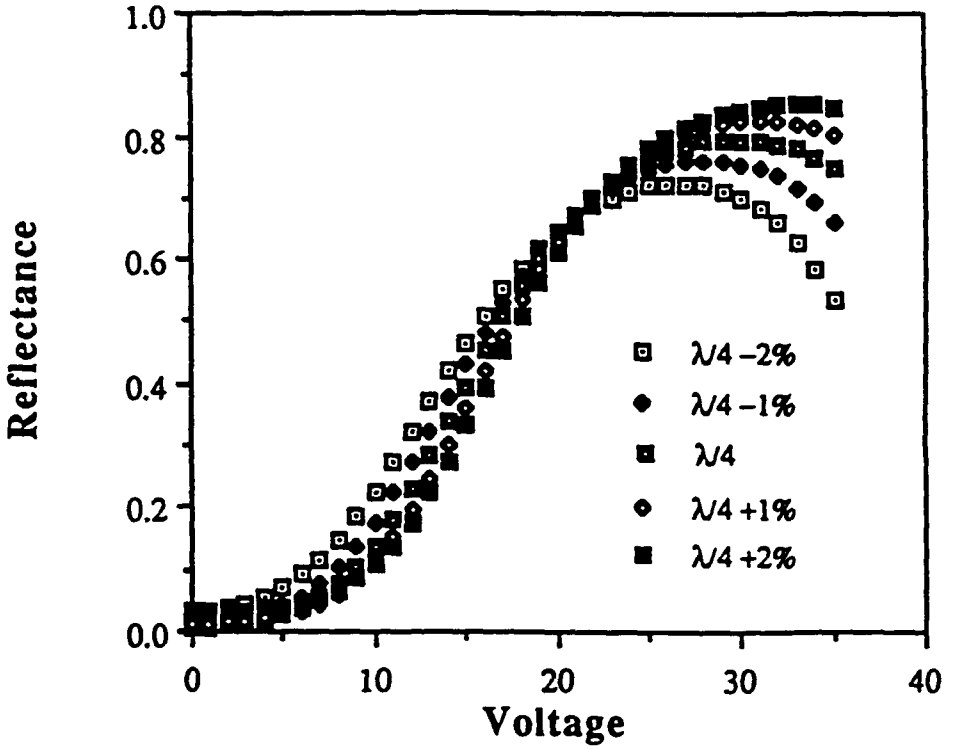

Figure 15. Variation of the reflectance of 8 pairs PBN/PLZT multilayer stack on silicon when the thickness of the individual layers deviates from their design values.

The 3 dB deviation from the center point for contrast ratio results in a thickness tolerance of 1.5%, one order of magnitude higher compared to MQW modulators. The wavelength operation region for this structure is approximately 75 nm centered at 514 nm. It is to note that for longer operating wavelengths such as 800 nm range, the thickness tolerance can be further increased. Additionally, we have to mention that there is no absorption in the off- state alleviating incoming power limitations. The deposition is also easier and more controllable by the incorporation of a simple reflectance monitor that would stop the deposition process when the null reflection has been obtained.

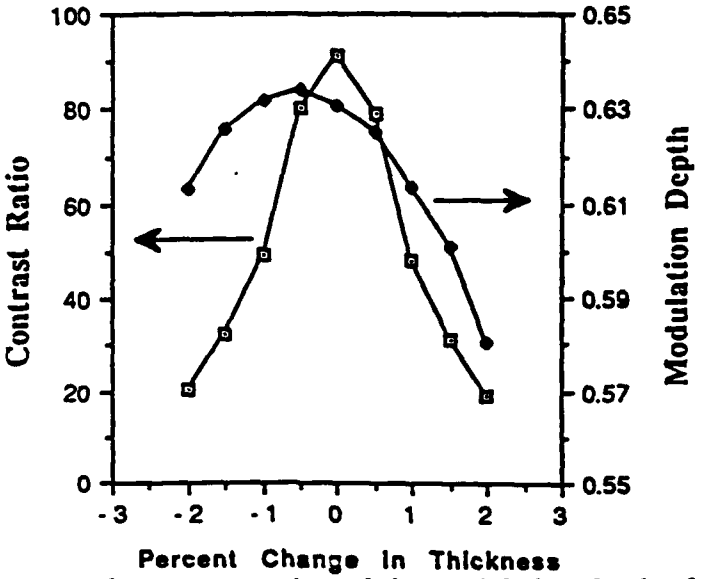

Figure 16. Tolerances on the contrast ratio and the modulation depth of 8 pairs PBN/PLZT multilayer stack on silicon with respect to the variation in the individual layer thickness. 3 dB point for contrast ratio defines a tolerance of about 1.5% from the design value.

B. Multilayer Design for Increased Contrast Ratio

The contrast ratio obtained from these simple multilayer films are limited due to reflection losses resulting from refraction index mismatch at the top and bottom of the stack. These mismatches yield a low (off) state reflectance value far from ideal zero case. These type of modulators can be used in application where the contrast ratio can be traded-in for relaxed wavelength and deposition thickness control. For application where contrast ratio is the primary concren, the contrast ratio can be further increased by achieving a better off-state value (null) without affecting the on -state by incorporating various material in the top and bottom of the stack.

B.1. Multilayer High Reflector Design

Multilayer high reflector design (HR) will consist of alternating many layers of ferroelectric layers such as PLZT (n = 2.55) and PBN (n = 2.32) designed for wavelength slightly greater than the wavelength of operation to enhance the reflection. The application of field shifts the pass- band of the stack toward the shorter wavelength as the optical path lengths of individual film layers decrease. A $\lambda/4$ thick SiO2 (n = 1.45) matching layer is placed on top of the stack to suppress the reflectance null (at V = 0) from 0.046 to 0.00016. Reflectance of the stack formed by 17 layers for operation at λ_o = 514.5nm varies from 0.00016 to 0.8967 for applied voltage variation from 0 to 30V; this corresponds to contrast >5000. The contrast ratio suffers -3dB reduction when wavelength deviates 0.06 nm from the center wavelength λ_o;

whereas the null at V = 0 increases to 0.00032. The structure tolerates 2.2 ° incident angle variation at λ_o before the contrast suffers -3dB reduction. The reflectance as a function of applied voltage at λ_o = 514.5 nm for a typical HR stack is calculated in Figure 17. A smooth transition from low reflectance (0.00) to high reflectance (>0.90) is readily obtainable for voltage swing of ~40 V. High-pass multilayer filter design is being evaluated as a possible solution to increase the wavelength tolerance.

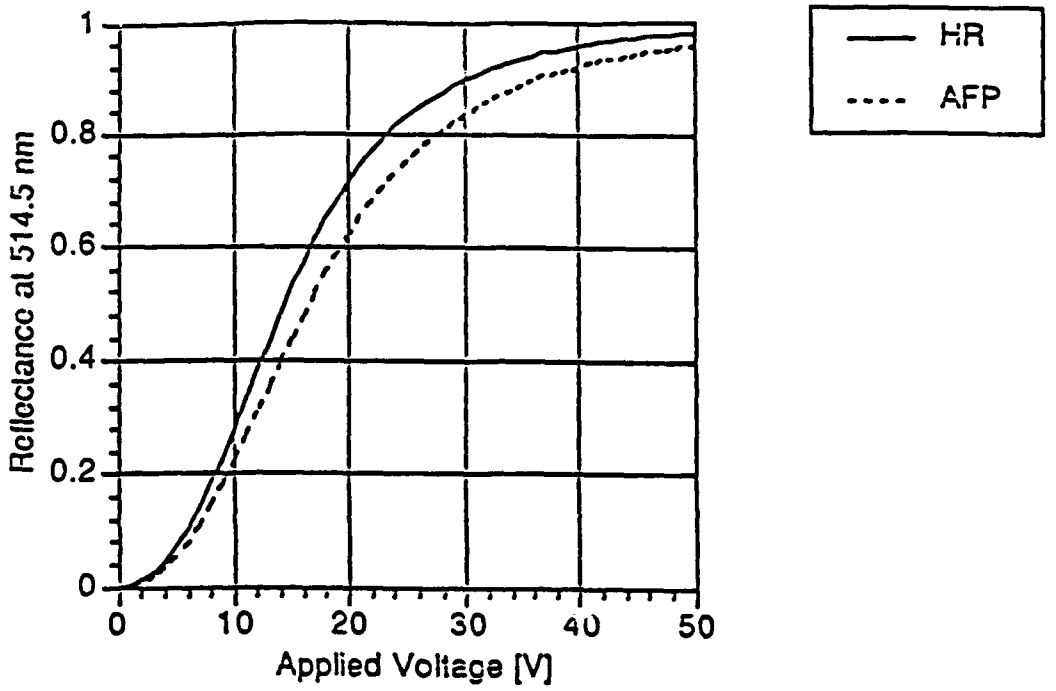

Figure 17. Radiant reflectance vs. applied voltage at λ = 514.5 for high reflectance (HR) and assymmetric Fabry-Perot (AFP) multilayers.

B.2. Multilayer Asymmetric Fabry-Perot Design

Another way to increase the contrast ratio is to place the multilayer structure in an asymmetric Fabry-Perot structure (AFP). A typical AFP structure is illustrated in Figure 18. With AFP stacks, thickness of the spacer layer becomes an additional parameter to control the characteristics of the multilayer stack. The null value of AFP stack may also be suppressed by adding a top layer (e.g. $\lambda/4$ thick AlF_3 n = 1.38) to enhance the matching of reflectivities on opposite sides of the spacer layer. Addition of this layer suppresses the reflectance null from 0.00125 to 0.00043. The upper mirror is formed by 12 layers and the bottom mirror has 19 layers.jjjjj Total thickness of the stack is about 3.6 μm. The reflectance as a function of applied voltage at λ_o = 514.5 for a typical AFP stack is calculated in Figure 17. A smooth transition from low reflectance (0.00) to high reflectance (>0.90) is again obtainable for voltage swing of

-40 V. Radiant reflectance for λ = 514.5 of the stack varies from 0.00043 to 0.8363 for applied voltage variation from 0 to 30V; this corresponds to contrast of 2000:1. Simulations indicate that such a structure can tolerate wavelength variation of 0.5 nm before suffering -3dB decrease in contrast; this occurs consequently as the null (at V = 0) increases to 0.00089. The AFP modulator design tolerates 1.55 ° incident angle variation before contrast suffers -3dB reduction. AFP stack may offer better wavelength tolerance than the HR stack at the cost of increased overall thickness.

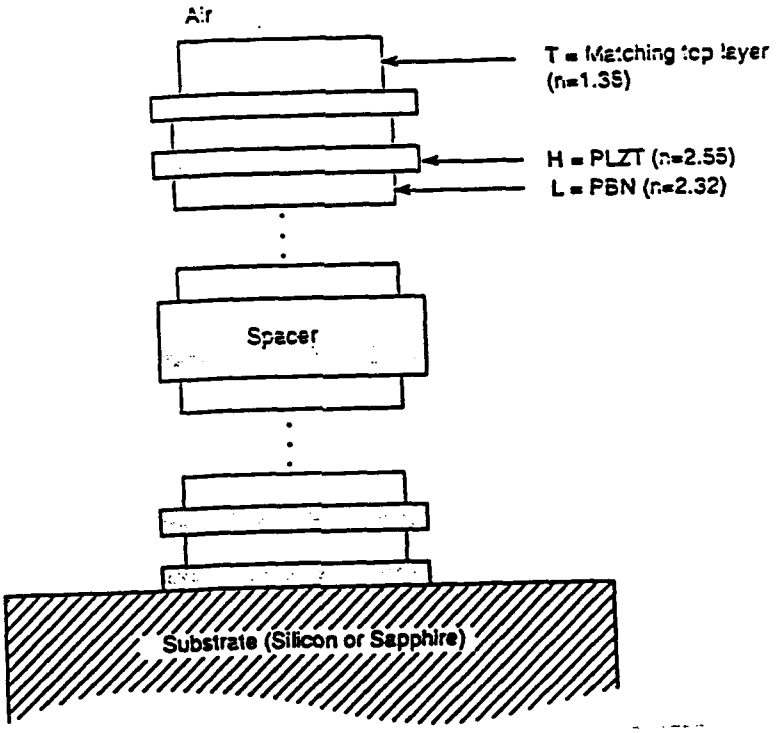

Figure 18. Asymmetric Fabry-Perot modulator structure incorporating ferroelectric PLZT and PBN layers. Additional $\lambda/4$ thick layer on the top of the active layer supresses the null further.

Although the initial calculations omitted some critical effects such as slight absorption, dispersion and interface scattering, the simulation results are promising. The material selection in terms of constituents of the multilayer stack, the number of layer pairs, operating wavelength, index of refraction of the consituents, the selection of substrate , the selection of interface layers to enhance the reflection/transmission between the substrate and the multilayer stacks are all parameter affecting the optimization. Further material deposition and characterization efforts are needed for a better optimization and for the realization of this promising thin film modulator type.

APPLICATION TO RECONFIGURATION AND MEMORY

Optically induced refractive index changes (photorefractive effect) in ferroelectric crystal have been widely used in volume holographic recording and real-time wave mixing, which are the basis of many photorefractive applications such as holographic memories, optical interconnects and optical correlators [20]. The general requirements for the photorefractive applications are high sensitivity to allow parallel processing at low optical powers, large and uniform gain and refrative index modulation to allow processing of wide spatial frequency signals, high resolution and large aperture size of optical quality to process images of large space bandwitdh product, fast response time, long storage time and large storage capacities for memories. Bulk ferroelectric materials have limited size: most common crystals such as $BaTiO_3$ or SBN are only available in few centimeter sizes. Photorefrative thin films offer the advantage of large optical aperture and can be deposited on host substrates for packaging and integration purposes. Therefore, the space-bandwidth product of the system utilizing these thin films can be improved. The diffraction efficiency of a hologram recorded in thin film with a thickness of a few microns will be three or four order magnitude smaller than that of the volume hologram with few millimeters thickness. One way to increase the diffraction efficiency of the hologram recorded in the thin film is to increase the effective thickness of the hologram which can be done by simply stacking many thin films together [21]. Another way is to increase the magnitude of the space charge field tyhat generates the index modulation via electro-optic effects. This can be achieved by recording the hologram in large grating spacing and applying an external DC field. Taking the SBN:60 as an example, with the grating spacing of 20 μm and an applied field of 50 KV/cm, a diffraction efficiency of 1% can be obtained in a film thickness of 5 μm. Thin film with periodic electrodes, as shown in Figure 19, can be utilized for field enhancement.

Recently a non-holographic memory application of a ferroelectric thin films have been disclosed [22]. In this application, an electrical field is used to change the polarization state of the thin film (write) and the change is read optically in a PLZT thin film deposited on a disk. The resulting ferroelectric optical disk (FOD) is expected to offer several orders of magnitude higher sotrage capacity than traditional hard disks and can be rewritten more than a million times.

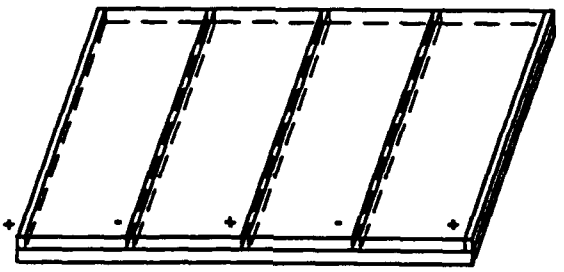

Figure 19. Thin ferroelectric photorefractive film with periodic electrodes for holographic memory applications.

CONCLUSIONS

Ferroelectric oxide materials such as PLZT, SBN, KTN, and PBN can serve useful as electro-optic elements for smart pixel applications. Towards this end, thin films of PLZT (9/65/35) have been grown on substrates such as sapphire, silicon, and platinum. These films show electro-optic effects with a quadratic E-O coefficient of 0.6×10^{-16} m^2/V^2. To provide the required contrast ratios for optoelectronic system needs, new geometries enhancing the electro-optic effects in these films have been proposed. One such geometry is the Fabry-Perot light modulator. This modulation enhances the electro-optic effect in these films by increasing the effective optical path through the material. Another approach is to grow multilayers of dissimilar electro-optic materials. The difference in index between the layers generates enhanced electro-optic effects. Simulations have been performed on both the proposed light modulator geometries. We have modeled the contrast ratios while varying the thickness and properties of the structure. Both these structures are very promising for S-SLM needs. Ferroelectric thin films are also promising for holographic and non-holographic memory and reconfiguration applications.

ACKNOWLEDGEMENTS

This work has been supported by the Defense Advanced Research Project Agency through Air Force Office of Scientific Research.

REFERENCES

1. M. Murdocca, A. Huang, J. Johns, and N. Streibl, *Applied Optics*, 27, pp. 1651-1658 (1988).
2. F. Kiamilev, S. Esener, R. Paturi, Y. Fainman, C. Guest, and S. H. Lee, *Opt. Eng.*, 28, pp. 396-409 (1989).
3. J. Neff, R. Athale and S. H. Lee, *Proc. IEEE*, 78 (5), pp. 826-855 (1990).
4. Tsen-Hwang Lin, A. Ersen, J. H. Wang, S. Dasgupta, S. Esener and S. H. Lee, *Applied Optics*, 29, No. 11, p. 1595 (1990).
5. Y. Fainman, Spatial Light Modulators and Applications III *Proc. SPIE*, U. Efron Ed., pp. 120-144 (1989).
6. J. Ford, Y. Taketomi, S. H. Lee, D. Bize, R. Neurgaonkar and Y. Fainman, *Proc. SPIE*, 1148 (1989).
7. J. Ma, J. Ford, Y. Taketomi, and S. H. Lee, *Opt. Lett.*, 16 (4), pp. 270-272, (1991).
8. J. Goodman, F. Leonberger, S. Kung and R. Athale, *Proc. IEEE*, 72 (7), pp. 850-866 (1984).
9. M. Feldman, S. Esener, C. Guest, and S. H. Lee, *Applied Optics*, 27, pp. 1762-1751 (1988).
10. F. Kiamilev, P. Marchand, A. Krishnamoorthy, S. Esener, and S. H. Lee, *IEEE J. Lightwave Technology*, 9, pp. 1674-1692 (1991).
11. A. Ersen, S. Krishnakumar, V. Ozguz, J. Wang, C. Fan, S. Esener and S. H. Lee, *Applied Optics*, 31, pp. 3950-3965,(1992).
12. S. Krishnakumar, V. H. Ozguz, C. Fan, S. Esener and S. H. Lee, *IEEE Tran. Ultrasonics, Ferroelectrics and Frequency Control*, 38, pp. 585-590 (1991).
13. M. Ishida, H. Matsunami and T. Tanaka, *J. Appl. Phys.*, 15, pp. 951-953 (1977).
14. G. H. Haertling and C. E. Land, *J. Am. Ceram. Soc.*, 54, pp 1-11, (1971).
15. M. DiDomenico Jr., S. H. Wemple, *J. Appl. Phys.* 40, pp. 720-732 (1969).
16. C. J. Kirkby, *Ferroelectrics* 7, pp. 157-159 (1974).
17. M. Okuyama, T. Usuki, Y. Hamakawa, T. Nakagawa, *Applied Physics* 21, pp. 339-343 (1980).
18. H. Adachi,T. Mitsuyu, O. Yamazaki, K. Wasa, *J. Appl. Phys.*, 60, pp. 736-741 (1986).
19 K. K. Law, J. L. Merz and L. Coldren, *J. applied Physics*, 72, (3), pp. 855-860, 1992.
20. Y. Fainman, J. Ma and S. H. Lee, *Materials Science Reports*, 9, pp. 53-139 (1993).

21. G. Gordin and A. Tanguay Jr, *Opt. Lett.*, pp. 1709-1711 (1992).
22. U.S. Patent No. 5,179,533 asssigned to Radiant Technologies Inc.